ISSCR

OPEN ACCESS

Mthfd2 Modulates Mitochondrial Function and DNA Repair to Maintain the Pluripotency of Mouse Stem Cells

Liang Yue,[1,2] Yangli Pei,[1,3] Liang Zhong,[1,4] Henry Yang,[5] Yanliang Wang,[1] Wei Zhang,[1] Naixin Chen,[1] Qianqian Zhu,[1] Jie Gao,[1] Minglei Zhi,[1] Bingqiang Wen,[1] Shaopeng Zhang,[1] Jinzhu Xiang,[1] Qingqing Wei,[1] Hui Liang,[1] Suying Cao,[6] Huiqiang Lou,[1] Zhongzhou Chen,[1] and Jianyong Han[1,2,*]

[1]State Key Laboratory for Agrobiotechnology, College of Biological Sciences, China Agricultural University, Beijing 100193, China
[2]Advanced Innovation Center for Food Nutrition and Human Health, China Agricultural University, Beijing 100083, China
[3]School of Life Science and Engineering, Foshan University, Foshan, Guangdong 528231, China
[4]Hebei Provincial Key Laboratory of Basic Medicine for Diabetes, The Shijiazhuang Second Hospital, Shijiazhuang, Hebei 050051, China
[5]Cancer Science Institute of Singapore, National University of Singapore, Singapore 117599, Singapore
[6]Animal Science and Technology College, Beijing University of Agriculture, Beijing 102206, China
*Correspondence: hanjy@cau.edu.cn
https://doi.org/10.1016/j.stemcr.2020.06.018

SUMMARY

The pluripotency of stem cells determines their developmental potential. While the pluripotency states of pluripotent stem cells are variable and interconvertible, the mechanisms underlying the acquisition and maintenance of pluripotency remain largely elusive. Here, we identified that methylenetetrahydrofolate dehydrogenase (NAD$^+$-dependent), methenyltetrahydrofolate cyclohydrolase (*Mthfd2*) plays an essential role in maintaining embryonic stem cell pluripotency and promoting complete reprogramming of induced pluripotent stem cells. Mechanistically, in mitochondria, *Mthfd2* maintains the integrity of the mitochondrial respiratory chain and prevents mitochondrial dysfunction. In the nucleus, *Mthfd2* stabilizes the phosphorylation of EXO1 to support DNA end resection and promote homologous recombination repair. Our results revealed that *Mthfd2* is a dual-function factor in determining the pluripotency of pluripotent stem cells through both mitochondrial and nuclear pathways, ultimately ensuring safe application of pluripotent stem cells.

INTRODUCTION

Pluripotent stem cells (PSCs), including embryonic stem cells (ESCs) and induced pluripotent stem cells (iPSCs), can self-renew or potentially differentiate into all cell types, a phenomenon known as pluripotency (Evans and Kaufman, 1981; Takahashi and Yamanaka, 2006). PSCs hold great promise for basic biomedical research, the production of genetically modified animals, and future clinical applications. Distinct pluripotent states, termed naive and primed pluripotency, have been described (Nichols and Smith, 2009). Naive PSCs resemble the preimplantation embryo inner cell mass (Boroviak et al., 2015) while primed PSCs resemble postimplantation embryonic epiblasts (Tesar et al., 2007). These states are reversible and interconvertible. The pluripotency of PSCs is known to determine the fate of embryonic development, and high-quality PSCs can produce chimeras with high efficiency when they are introduced into a blastocyst (Huang et al., 2012) and can develop into viable offspring by tetraploid complementation (Zhao et al., 2009; Zhong et al., 2019). Understanding the molecular mechanisms that influence pluripotency acquisition and maintenance is key to advancing therapeutic applications of PSCs.

Cells produce ATP by exploiting glycolysis and oxidative phosphorylation (OXPHOS) in different proportions to obtain energy for survival. Somatic cell reprogramming resets cellular metabolism to a state of relatively high glycol-

ysis and low OXPHOS (Folmes et al., 2011). PSCs in a naive state are highly oxidative compared with primed cells. The progression from naive to primed pluripotency is characterized by a metabolic shift from OXPHOS to glycolysis (Zhou et al., 2012), and resetting primed pluripotent cells to a naive state necessitates a reversal of the metabolic switch (Carbognin et al., 2016; Takashima et al., 2014). Mitochondria are essential organelles in all nucleated cells that function mainly to generate cellular ATP by OXPHOS via the electron transport chain (ETC, complexes I–IV) and ATP synthase (complex V). Primed PSCs maintain lower mitochondrial function than naive cells (Zhang et al., 2016). In addition, the mitochondrial membrane potential (Sukumar et al., 2016), ATP (Zhang et al., 2018), reactive oxygen species (ROS) (Ryu et al., 2015; Zhou et al., 2016), and mitochondrial dynamics (Khacho et al., 2016; Zhong et al., 2019) were reported as the key factors responsible for cell-fate changes. However, the factors that determine mitochondrial function in PSCs and their regulatory mechanism remain unclear.

Genetic lesions of either endogenous or exogenous origin are major threats to the function of PSCs (Weissbein et al., 2014; Yoshihara et al., 2017). PSCs rely on a very robust DNA damage response (DDR) to detect and control specific types of DNA damage. Once DNA damage is unresolvable, PSCs avoid the propagation of genetic lesions by undergoing regulated cell death (Desmarais et al., 2016; Liu et al., 2013) or losing pluripotency (Li et al., 2012; Lin
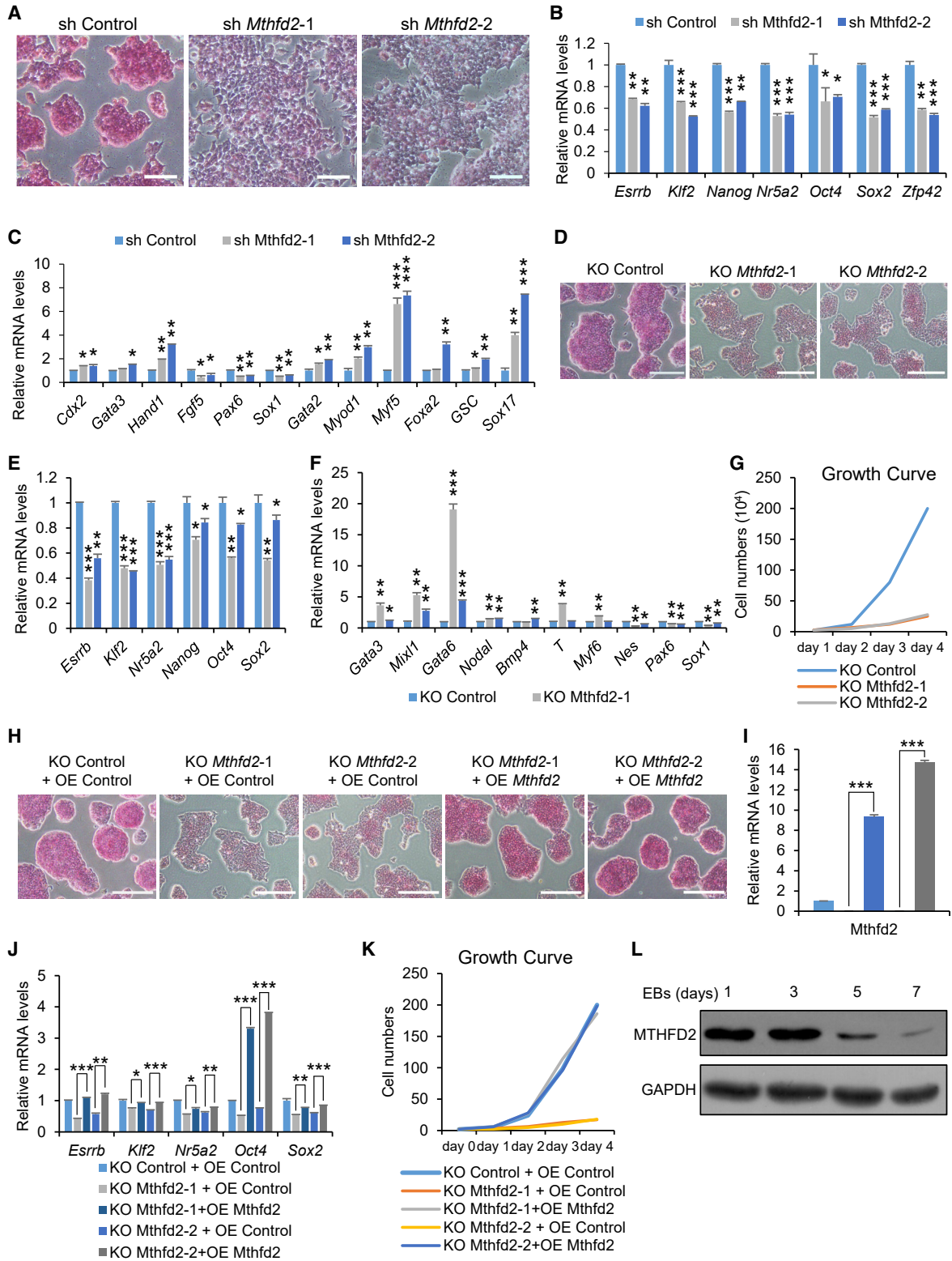
Figure 1. *Mthfd2* Is Important for mESCs to Maintain Self-Renewal

(A) Representative results of *Mthfd2* KD mESCs with AP staining. Scale bars, 100 μm.

(B and C) qRT-PCR analysis of mRNA levels of pluripotency marker genes (B) and lineage marker genes (C) in *Mthfd2* KD mESCs.

(legend continued on next page)

et al., 2005). Among all types of DNA lesions, DNA double-strand breaks (DSBs) are arguably the most dangerous (Jackson, 2002), and PSCs predominantly use homologous recombination (HR) to repair DSBs (Tichy et al., 2010). Failure of HR repair systems typically leads to severe consequences, such as genomic instability in cellular reprogramming (Gonzalez et al., 2013; Lee et al., 2016). Thus, efficacious DSB repair is a key element in the maintenance of high genomic integrity. However, the mechanisms that protect genomic integrity and the key regulators involved are not completely clear.

In this study, we identified methylenetetrahydrofolate dehydrogenase (NAD$^+$-dependent), methenyltetrahydrofolate cyclohydrolase (*Mthfd2*) as an important regulator of pluripotency in mouse PSCs. *Mthfd2* is a bifunctional enzyme with methylene dehydrogenase and cyclohydrolase activity involved in mitochondrial folate one-carbon metabolism (Tibbetts and Appling, 2010). *Mthfd2* plays an essential role in mouse embryonic development, because inactivation of this gene in mice was demonstrated to be lethal (Di Pietro et al., 2002). *MTHFD2* is markedly elevated in many cancers and positively correlated with poor prognosis in patients with cancer (Lin et al., 2018; Liu et al., 2014a; Pikman et al., 2016). In addition, *MTHFD2* is localized to the nucleus and affects proliferation independent of its enzymatic activity in cancer cells (Gustafsson Sheppard et al., 2015). However, the function of *Mthfd2* in PSCs has not been reported. Here, we demonstrated that *Mthfd2* mediates both mitochondrial function and DNA repair to determine the pluripotency state of PSCs, ultimately improving their potential use in various applications and their safety.

RESULTS

A Microarray Assay Identifies Putative New Pluripotency-Regulating Genes in iPSCs

We reanalyzed the microarray data from iPSCs of different quality initially generated in our laboratory and demonstrated the quality of the iPSCs based on their *in vitro* developmental potential (Han et al., 2010; Heng et al., 2010). High-quality iPSCs underwent germline transmission or produced mice derived completely from iPSCs by tetraploid complementation, while low-quality iPSCs produced only chimeras with a low coat color contribution. Candidate genes were selected based on their higher expression in high-quality iPSCs than in low-quality iPSCs (Table S1). Among these candidates, *Esrrb*, *Sall4*, *Gadd45a*, and *Rab32* were previously reported to be important for enhancing iPSC generation and modulating ESC pluripotency (Chen et al., 2016; Feng et al., 2009; Pei et al., 2015; Zhang et al., 2006). Besides, some new potential regulators such as *Mthfd2* were identified (Figure S1A).

### *Mthfd2* Plays a Key Role in Mouse ESCs to Maintain Self-Renewal

To validate the role of the candidate genes in regulating mouse ESC (mESC) self-renewal, we separately used short hairpin RNAs (shRNAs) to suppress the expression of candidate genes in E14 mESCs. *Mthfd2* knockdown (KD) resulted in loss of typical stem cell morphology (Figures S1B–S1D), with reduced alkaline phosphatase (AP) staining (Figure 1A). The expression of pluripotency marker genes was downregulated and that of lineage marker genes upregulated (Figures 1B, 1C, and S1E), showing that *Mthfd2* depletion results in differentiation of mESCs. We then knocked down *Mthfd2* in another G4 mESC line and found that the results were consistent with those in *Mthfd2* KD E14 mESCs (Figures S1F and S1G). Additionally, homozygous *Mthfd2* knockout (KO) mESCs were characterized by the loss of typical mESC morphology, abnormal expression of marker genes, and compromised cell proliferation (Figures 1D–1G and S1H). Forced expression of *Mthfd2* rescued the *Mthfd2* KO-induced differentiation and compromised cell proliferation (Figures 1H–1K). In addition, MTHFD2 protein expression was gradually silenced during the differentiation of mESCs into embryoid bodies (EBs) (Figure 1L). These results demonstrate a key role of *Mthfd2* in the maintenance of mESC self-renewal.

Mthfd2 Facilitates Mouse iPSC Induction

We used *Oct4*, *Sox2*, and *Klf4* (OSK) combined with various candidate factors, including *Mthfd2*, in a subsequent

(D) Representative results of *Mthfd2* KO mESCs with AP staining. Scale bars, 200 μm.

(E and F) qRT-PCR analysis of mRNA levels of pluripotency marker genes (E) and lineage marker genes (F) in *Mthfd2* KO mESCs.

(G) Representative growth curve of *Mthfd2* KO mESCs.

(H) Representative results of overexpressed (OE) *Mthfd2-Mthfd2* KO mESCs with AP staining. Scale bar, 200 μm.

(I and J) qRT-PCR analysis of mRNA levels of *Mthfd2* (I) and pluripotency marker genes (J) in OE *Mthfd2-Mthfd2* KO mESCs.

(K) Representative growth curve of OE *Mthfd2-Mthfd2* KO mESCs.

(L) Western blot analysis of the levels of the MTHFD2 protein during differentiation of mESCs. GAPDH was used as a loading control.

Data in (B), (C), (E), (F), (I) and (J) are pooled from three independent experiments (mean ± SD) relative to EF1-α and the control mESCs. *p < 0.05, **p < 0.01, ***p < 0.001 (Student's t test) compared with the control.

See also Figure S1.
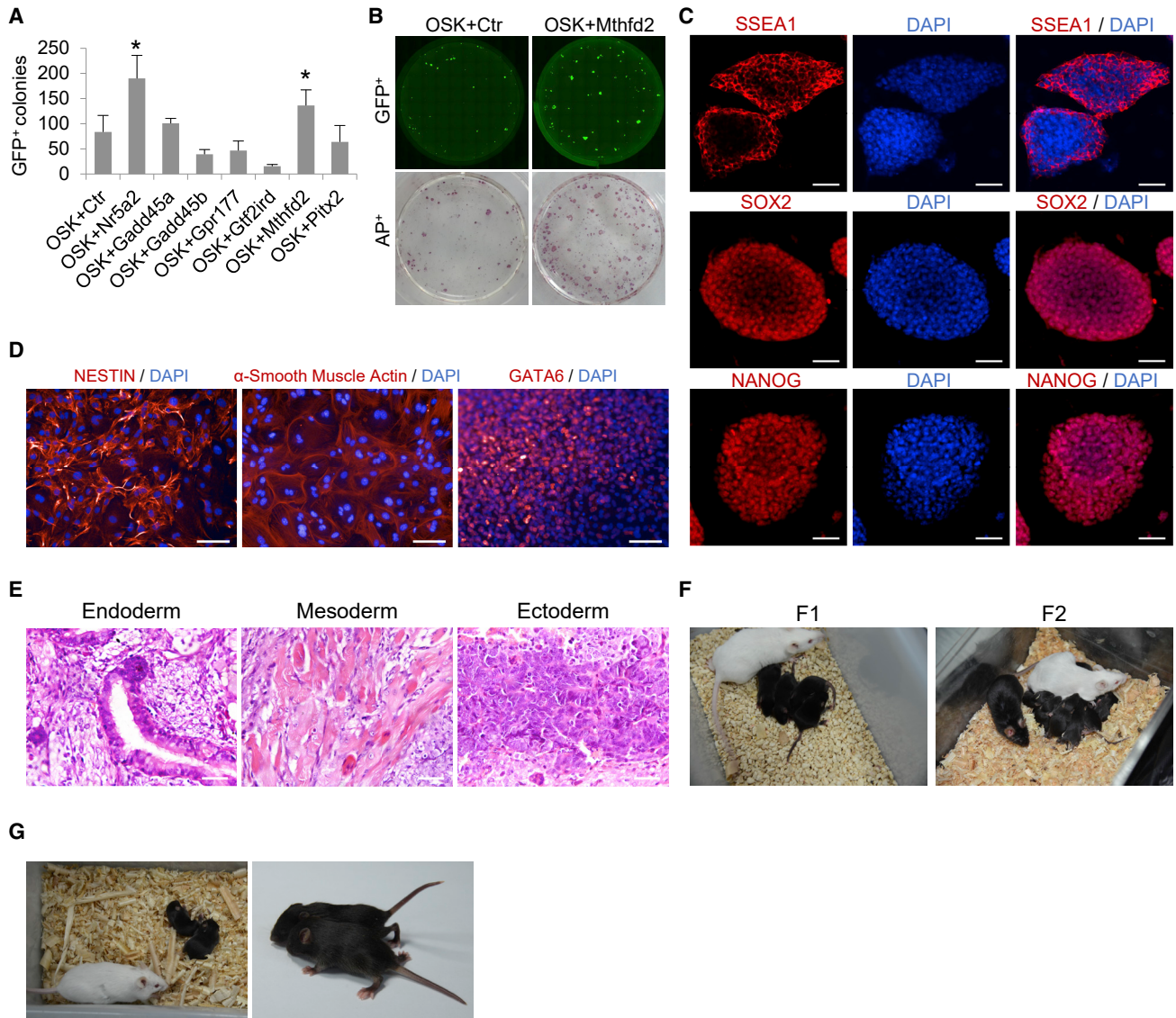
Figure 2. *Mthfd2* Promotes Complete Reprogramming of iPSCs

(A) The reprogramming efficiencies in KOSR medium. OSK + control (Ctr) cells were used as a control. Data are pooled from three independent experiments (mean ± SD). *p < 0.05, **p < 0.01, ***p < 0.001 (Student's t test) compared with the control.

(B) Full-well mosaic images of Oct4-GFP⁺ cells and AP⁺ colonies are shown for OSK+Ctr and OSKM2 iPSCs in KOSR medium.

(C) Immunofluorescence (IF) staining for pluripotency marker proteins in OSKM2 iPSCs. DAPI was used to indicate the nuclei. Scale bars, 100 μm.

(D) IF staining for GATA6 (endoderm), NESTIN (ectoderm), and α-smooth muscle actin (mesoderm) in EBs derived from OSKM2 iPSCs. DAPI was used to indicate the nuclei. Scale bars, 100 μm.

(E) H&E staining of teratomas derived from OSKM2 iPSCs. Scale bars, 100 μm.

(F) Representative images of chimeric mice (F1) and their offspring (F2).

(G) Live-born pups obtained from OSKM2 iPSCs were tested by tetraploid complementation.

See also Figure S2.

reprogramming assay (Takahashi and Yamanaka, 2006). Mouse embryonic fibroblasts (MEFs) expressing a green fluorescent protein (GFP) reporter driven by an *Oct4* promoter and enhancer (termed OG2 MEFs) were used for iPSC induction. To ensure the reliability of our results, we tested two culture conditions, serum + LIF (leukemia inhibitory factor) mESC medium and KOSR medium, the latter of which has been reported to enhance iPSC induction
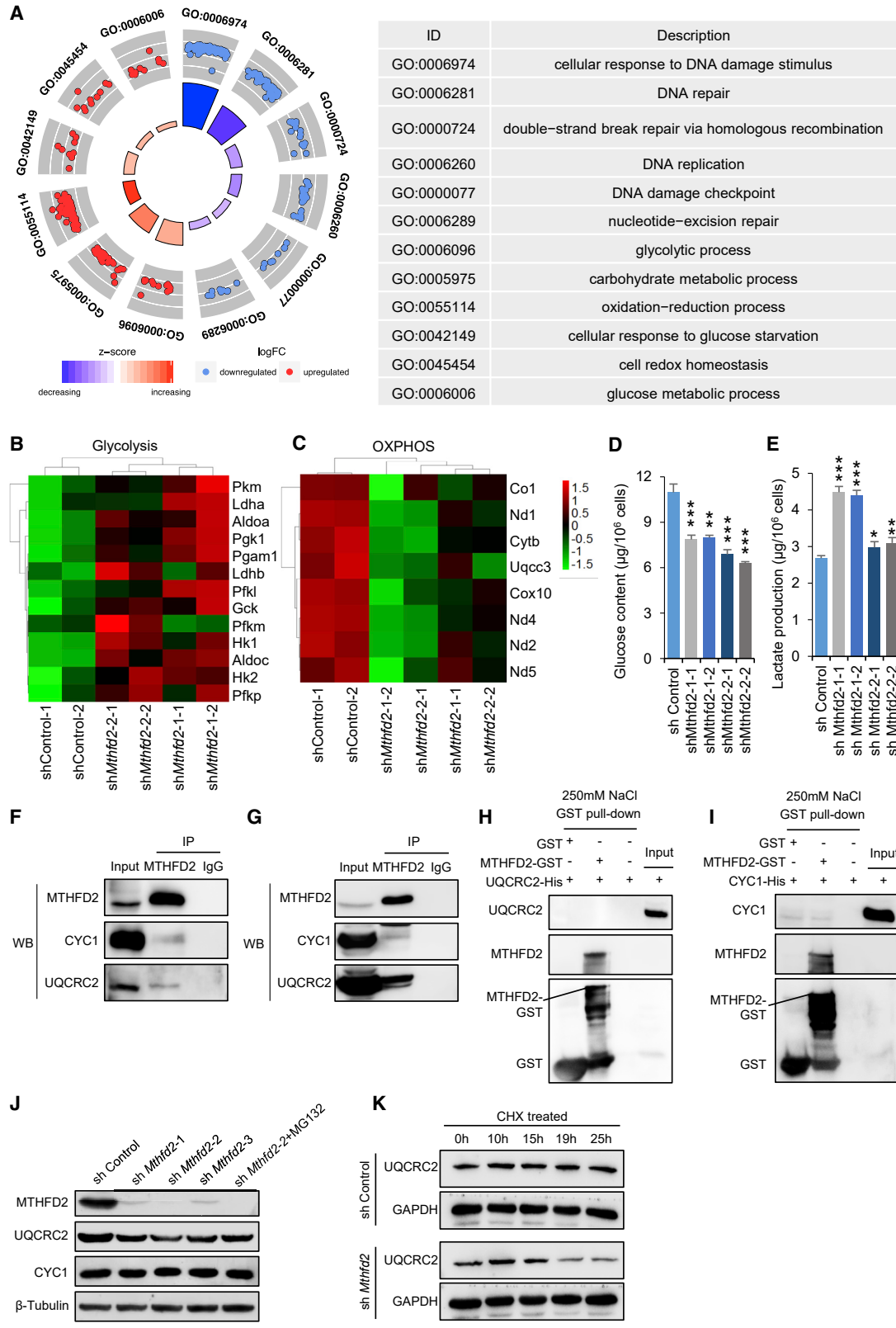
(legend on next page)

(Liu et al., 2014b). The number of Oct4-GFP⁺ colonies generated by coinfection of *Mthfd2* and OSK was increased approximately 2-fold relative to that in control cells which coinfection of empty vector and OSK (p < 0.05) in both mESC medium (Figures S2A and S2B) and KOSR medium (Figures 2A and 2B). We used doxycycline-inducible MEFs expressing *Oct4*, *Sox2*, *Klf4*, and *c-Myc* (OSKC) reprogramming factor TF4 (Gao et al., 2013) for reprogramming to further confirm the *Mthfd2*-mediated improvements. The number of AP⁺ colonies was increased in the *Mthfd2*-overexpressing group compared with that in the control group (Figures S2C and S2D) (p < 0.05). These results indicated that *Mthfd2* facilitates the induction of iPSCs.

Mthfd2 Improves the Quality of iPSCs

All iPSCs induced with *Mthfd2* (OSKM2 iPSCs) showed typical mESC-like morphology and expressed Oct4-driven GFP (Figure S2E). Exogenous retroviral expression of OSK and *Mthfd2* was silenced (Figure S2F), and the expression of pluripotency marker genes was similar in OSKM2 iPSCs and mESCs (Figure S2G). In addition, two master transcription factors (*Nanog* and *Sox2*) and the mESC-specific surface marker SSEA1 were expressed in OSKM2 iPSCs (Figure 2C).

We conducted EB and teratoma formation assays to assess the ability of OSKM2 iPSCs to differentiate *in vitro* and *in vivo*. The EBs and teratomas derived from OSKM2 iPSCs differentiated into cells of all three germ layers (Figures 2D and 2E). Furthermore, the developmental potential of OSKM2 iPSCs *in vivo* was tested via 8-cell embryo injection (Xiang et al., 2018), and chimeric mice derived almost completely from iPSCs were produced and had the ability of germline transmission (Figure 2F). Next, we tested the developmental potential of OSKM2 iPSCs *in vivo* by tetraploid complementation (Zhao et al., 2009). Remarkably, OSKM2 iPSCs gave rise to viable all-iPSC-derived pups (Figure 2G) with higher efficiency than control OSKC iPSCs (Figure S2H). Collectively, these results indicated that *Mthfd2* improves the quality of iPSCs.

Mthfd2 Depletion Shifts Glucose Metabolism from OXPHOS to Glycolysis in mESCs

MTHFD2 was reported to be an important enzyme in mitochondrial one-carbon metabolism (Tibbetts and Appling, 2010). Two MTHFD2-specific inhibitors, MIN and NIT (Asai et al., 2018), were used to inhibit MTHFD2 enzymatic activity in mESCs. Both MIN- and MIT-treated mESCs (MImESCs) maintained typical stem cell morphology and pluripotency-associated marker gene expression (Figures S3A–S3C). Therefore, we speculated that the MTHFD2 has nonenzymatic functions in mESCs. To characterize the global function of *Mthfd2* in mESCs, we analyzed changes in the transcriptome due to suppression of *Mthfd2* (Figure S3D and Table S2). Among the differentially expressed genes (DEGs), pluripotency-associated genes were downregulated in *Mthfd2* KD mESCs (Figure S3E). Interestingly, gene ontology (GO) terms such as glycolytic process were among the top ten terms enriched in upregulated genes (Figure S3F), and additional GO terms associated with carbohydrate metabolism were among the terms enriched in upregulated genes (p < 0.05) (Figure 3A). Glucose metabolism is a complex and dynamic process and is the most potent modulator of PSC pluripotency states and cell-fate changes (Carbognin et al., 2016; Shyh-Chang and Daley, 2015; Zhou et al., 2012). Subsequently, we evaluated whether the cellular glucose metabolism state was altered in *Mthfd2* KD mESCs. Among the DEGs, the levels of key glycolytic genes were increased and those of some key OXPHOS genes were decreased in *Mthfd2* KD mESCs (Figures 3B and 3C). Lower intracellular glucose levels and higher intracellular lactate levels were detected in *Mthfd2* KD cells than in control cells (Figures 3D and 3E), indicating increased consumption of glucose and production of lactate in *Mthfd2* KD mESCs. Therefore, *Mthfd2* depletion shifts glucose metabolism from OXPHOS to glycolysis in mESCs.

MTHFD2 Interacts with Mitochondrial ETC Complex III in Mitochondria

To understand the mechanism by which *Mthfd2* functions in mESCs, we used an immunoprecipitation and mass

---

Figure 3. MTHFD2 Interacts with Complex III to Regulate Glucose Metabolism in mESCs

(A) Summary of enriched GO terms that were potently upregulated and downregulated by *Mthfd2*. p < 0.05. For details, see Table S2.

(B and C) Heatmap of DEGs about glycolysis (B) and OXPHOS (C) between control mESCs and *Mthfd2* KD mESCs.

(D and E) Examination of intracellular glucose levels (D) and lactate levels (E) in *Mthfd2* KD mESCs. Data are pooled from three independent experiments (mean ± SD). *p < 0.05, **p < 0.01, ***p < 0.001 (Student's t test) compared with the control.

(F and G) CoIP results showing the specific interactions between endogenous MTHFD2 and both UQCRC2 and CYC1 in mESCs (F) and in the cytoplasm fraction of mESCs (G).

(H and I) GST pull-down assays for interaction between UQCRC2-His (H), CYC1-His (I), and MTHFD2-GST fusion proteins at 250 mM NaCl containing GST binding buffer.

(J) Western blot analysis of the levels of the UQCRC2 and CYC1 proteins in *Mthfd2* KD mESCs. β-Tubulin was used as a loading control.

(K) Western blot analysis of UQCRC2 protein in *Mthfd2* KD mESCs at indicated times post cycloheximide (CHX) treatment. GAPDH was used as a loading control.

See also Figures S3–S5.
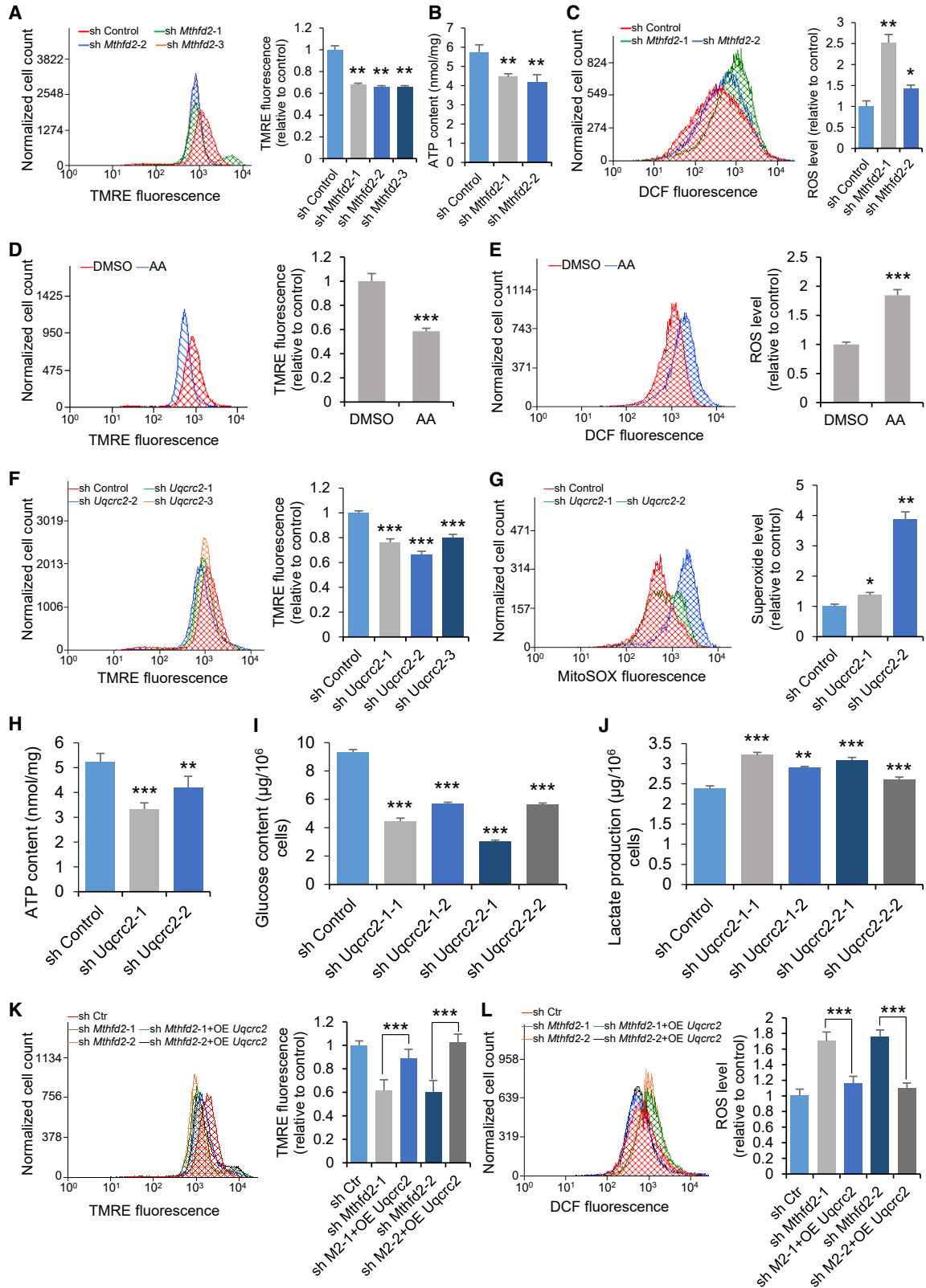
(legend on next page)

spectrometry (IP-MS) assay to search for proteins that interact with MTHFD2. MTHFD2 was localized to both the nucleus and mitochondria in mESCs (Figures S4A and S4B), and its function in mESCs, particularly in the nucleus, remains unknown. Hence, we separated nuclear and cytoplasmic fractions from Mthfd2-FLAG mESCs and subjected them to IP-MS (Figures S4C–S4F).

Among the identified MTHFD2 partners were the complex III members UQCRC2 and CYC1 (Figure S4G and Table S3). Complex III is a component of the mitochondrial ETC, via which OXPHOS is mediated to generate ATP in eukaryotic cells (Hatefi, 1985; Mitchell, 1975). Given the upregulation of glycolysis in Mthfd2 KD mESCs, the interaction between MTHFD2 and complex III was particularly interesting. First, the interaction between FLAG-tagged MTHFD2 and hemagglutinin (HA)-tagged UQCRC2 was verified in E14 mESCs by reciprocal coimmunoprecipitation (coIP) experiments (Figure S5A). The specific interactions between endogenously expressed MTHFD2 and both UQCRC2 and CYC1 were then verified in E14 mESCs (Figure 3F). We further verified that MTHFD2 formed protein complexes with UQCRC2 and CYC1 in the cytoplasmic fraction (Figure 3G). To address the questions of whether the interactions between MTHFD2 and those proteins were direct, we conducted glutathione S-transferase (GST) pull-down assays using recombinant proteins. No direct interaction between MTHFD2-GST and either UQCRC2-His or CYC1-His was detected (Figures 3H and 3I). Thus, these results provide evidence for an indirect interaction between MTHFD2 and complex III in mitochondria of mESCs.

The protein level of UQCRC2 were reduced in Mthfd2 KD mESCs compared with control mESCs (Figure S5B) but did not differ between MI-mESCs and control mESCs (Figure S5C). Treatment with a 26S proteasome inhibitor, MG132, efficiently prevented the Mthfd2 depletion-induced reduction in UQCRC2 expression (Figure 3J). By treating cells with the protein synthesis inhibitor cycloheximide, we found that the half-life of UQCRC2 was consid-

erably shortened upon depletion of Mthfd2 (Figure 3K). Thus, Mthfd2 might play a role in maintaining the stability of the UQCRC2 protein.

Mthfd2 Deficiency Induces Mitochondrial Dysfunction by Regulating the Activity of Complex III

The main function of complex III is to transfer electrons between ubiquinol and cytochrome c, thus generating an electrochemical potential that drives ATP synthesis (Crofts, 2004). In addition, complex III is the major site of ROS generation (Chen et al., 2003). The mitochondrial membrane potential (MMP) and ATP production were decreased (Figures 4A and 4B) and cellular ROS levels were increased in Mthfd2 KD mESCs (Figure 4C). These effects are consistent with those observed in cells treated with antimycin A (a complex III inhibitor), which impairs mitochondrial function (Figures 4D and 4E), and indicated that Mthfd2 deficiency induces mitochondrial dysfunction in mESCs.

The mitochondrial dysfunction induced by Mthfd2 depletion resembled the phenotype observed in cells with Uqcrc2 deficiency, which leads to complex III deficiency (Aguilera-Aguirre et al., 2009; Miyake et al., 2013). Uqcrc2 KD cells exhibited reduced MMP and ATP production, increased levels of superoxide (a major ROS generated in mitochondria), and a shift of glucose metabolism to glycolysis (Figures 4F–4J). Moreover, forced expression of Uqcrc2 effectively rescued the Mthfd2 KD-induced changes in the MMP (Figure 4K) and the cellular ROS level (Figure 4L). In addition, the cellular ROS level (Figure S5D) and the MMP (Figure S5E) did not differ between MI-mESCs and control mESCs. Therefore, Mthfd2 depletion induces mitochondrial dysfunction through inhibition of complex III activity caused by a decrease in UQCRC2 expression.

Mthfd2 Depletion Hinders DNA Repair in mESCs

In addition to GO terms related to glycolysis, GO terms such as DNA repair were among the top ten terms

Figure 4. Mthfd2 Deficiency Induces Mitochondrial Dysfunction by Reducing Uqcrc2 Expression
(A) Measurements of the mitochondrial membrane potential (MMP) in Mthfd2 KD mESCs using tetramethylrhodamine methyl ester (TMRE).
(B) Total ATP levels in Mthfd2 KD mESCs.
(C) Flow-cytometry analysis of ROS levels in Mthfd2 KD mESCs.
(D) Measurements of the MMP in antimycin A-treated mESCs (AA-mESCs) using TMRE.
(E) Flow-cytometry analysis of ROS levels in AA-mESCs.
(F) Measurements of the MMP in Uqcrc2 KD mESCs using TMRE.
(G) Flow-cytometry analysis of superoxide levels in Uqcrc2 KD mESCs.
(H) Total ATP levels in Uqcrc2 KD mESCs.
(I and J) Examination of intracellular glucose levels (I) and lactate levels (J) in Uqcrc2 KD mESCs.
(K) Measurements of the MMP in OE Uqcrc2-Mthfd2 KD mESCs using TMRE.
(L) Flow-cytometry analysis of ROS levels in OE Uqcrc2-Mthfd2 KD mESCs.
All data are pooled from three independent experiments (mean ± SD). *p < 0.05, **p < 0.01, ***p < 0.001 (Student's t test) compared with the control. A representative histogram (left) and quantification of the mean fluorescence intensity (right) are presented for (A), (C) to (G), (K), and (L). See also Figure S5.
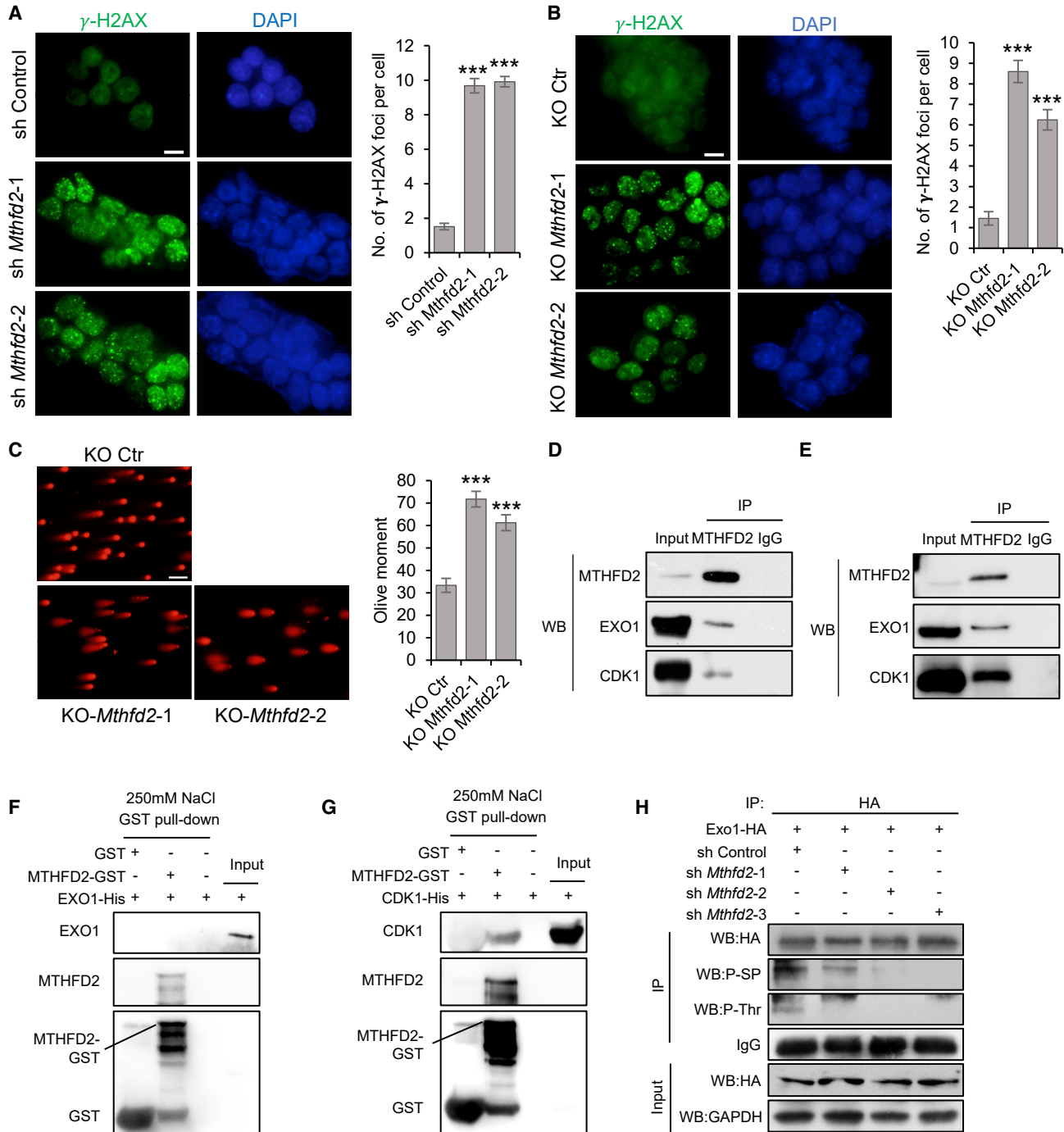
Figure 5. MTHFD2 Interacts with CDK1 and EXO1 to Regulate DNA Damage Level in mESCs

(A and B) IF staining for γ-H2AX in *Mthfd2* KD mESCs (A) *and Mthfd2* KO mESCs (B). Representative images (left) and quantification of the average number of γ-H2AX foci per cell (right) (n = 50 nuclei) are shown. DAPI was used to indicate the nuclei. Scale bar, 10 μm.

(C) DNA damage levels of *Mthfd2* KO mESCs were evaluated by the comet assay. Representative images (left) and quantification of the mean olive tail moment (right) (n = 50 nuclei) are shown. Scale bar, 100 μm.

(D and E) CoIP results showing the specific interactions between endogenous MTHFD2 and both CDK1 and EXO1 in mESCs (D) and in the nuclear fraction of mESCs (E).

(legend continued on next page)

enriched in downregulated genes (Figure S6A), and additional terms such as double-strand break repair via HR were enriched in downregulated genes (p < 0.05) (Figure 3A). PSCs rely on a very robust DNA repair response to control DNA damage, and if DNA damage is unresolvable, PSCs prevent the propagation of genetic lesions by undergoing regulated cell death (Liu et al., 2013) or losing pluripotency (Li et al., 2012; Lin et al., 2005). Therefore, we examined whether *Mthfd2* deficiency altered DNA damage levels in mESCs. Among the DEGs, DNA repair-associated genes exhibited decreased expression in *Mthfd2* KD mESCs (Figure S6B). Phosphorylation of H2AX (termed γ-H2AX) is one of the earliest events to occur following DNA DSB induction and is critical for protecting the genome from DSBs (Rogakou et al., 1998). Interestingly, the number of γ-H2AX foci increased substantially in *Mthfd2* KD mESCs (Figure 5A) and *Mthfd2* KO mESCs (Figure 5B) with increased passaging. The increase in DNA damage in *Mthfd2* KO mESCs was further validated by comet assay, a method that measures the extent of DNA damage on a single-cell basis (Figure 5C). These increases suggested that DNA damage accumulates following *Mthfd2* depletion.

MTHFD2 Interacts with CDK1 and EXO1 in the Nucleus

Under normal conditions, PSCs accurately repair DSBs mostly through the HR pathway (Tichy et al., 2010). EXO1 and CDK1, which play key roles in DNA HR repair (Tomimatsu et al., 2014), were detected among the identified MTHFD2 partners (Figure S4G and Table S3). Thus, we explored the interactions between MTHFD2 and both EXO1 and CDK1. The interactions between endogenously expressed MTHFD2 and both CDK1 and EXO1 were confirmed by coIP experiments (Figure 5D). We further verified that MTHFD2 interacts with both EXO1 and CDK1 in the nuclear fraction (Figures 5E and S6C). Moreover, a direct interaction between MTHFD2-GST and CDK1-His was detected by GST pull-down assays (Figures 5F and 5G). These results provide evidence for the interaction of CDK1 and EXO1 with MTHFD2 in the nucleus of mESCs. In addition, the interactions between MTHFD2 and UQCRC2, CYC1, CDK1, and EXO1 remained detectable in MI-mESCs (Figure S6D), emphasizing that the MTHFD2's interactions are not affected by its enzymatic activity.

During HR repair, EXO1 is primed to function in resection by CDK-mediated phosphorylation (Tomimatsu et al., 2014). We assessed the level of CDK1-induced EXO1 phosphorylation in *Mthfd2* KD mESCs. EXO1 phosphorylation was significantly reduced in *Mthfd2* KD mESCs compared with that in control mESCs (Figure 5H). Collectively, these results indicate that *Mthfd2* plays an important role in maintaining the phosphorylation of EXO1 in mESCs.

Mthfd2 Modulates HR Repair by Regulating EXO1 Phosphorylation

To understand whether the increased DNA damage in *Mthfd2* KD mESCs was caused by defects in DNA repair, we quantified and compared γ-H2AX foci formation after treatment with camptothecin (CPT), which induces DSBs (Hsiang et al., 1989). A significant reduction in DNA repair efficiency was observed in *Mthfd2* KD mESCs (Figures 6A, 6B, S6E, and S6F) and *Exo1* KD mESCs (Figures 6C, 6D, and S6G) after CPT treatment, consistent with a previous report that *Exo1* deletion impairs HR repair (Schaetzlein et al., 2007). This pattern was consistent with that observed in cells treated with RO-3306 (a specific CDK1 inhibitor), which hinders DNA repair and increases DNA damage (Figures 6E and 6F). Moreover, the comet assay results showed that forced expression of *Cdk1* effectively rescued the *Mthfd2* KD-induced impairment in DNA repair (Figure 6G). However, DNA damage level did not differ between MI-mESCs and control mESCs (Figures S6H and S6I), highlighting a key role of EXO1 phosphorylation in *Mthfd2*-mediated functions during DNA repair. Moreover, *Mthfd2* KD mESCs exhibited fewer Rad51 foci, a key component of HR repair, than control cells after CPT treatment, suggesting attenuation of HR repair (Figures 6H and 6I). These results revealed that *Mthfd2* regulates EXO1 phosphorylation by affecting the kinase activity of CDK1 to modulate HR repair and protect genomic integrity.

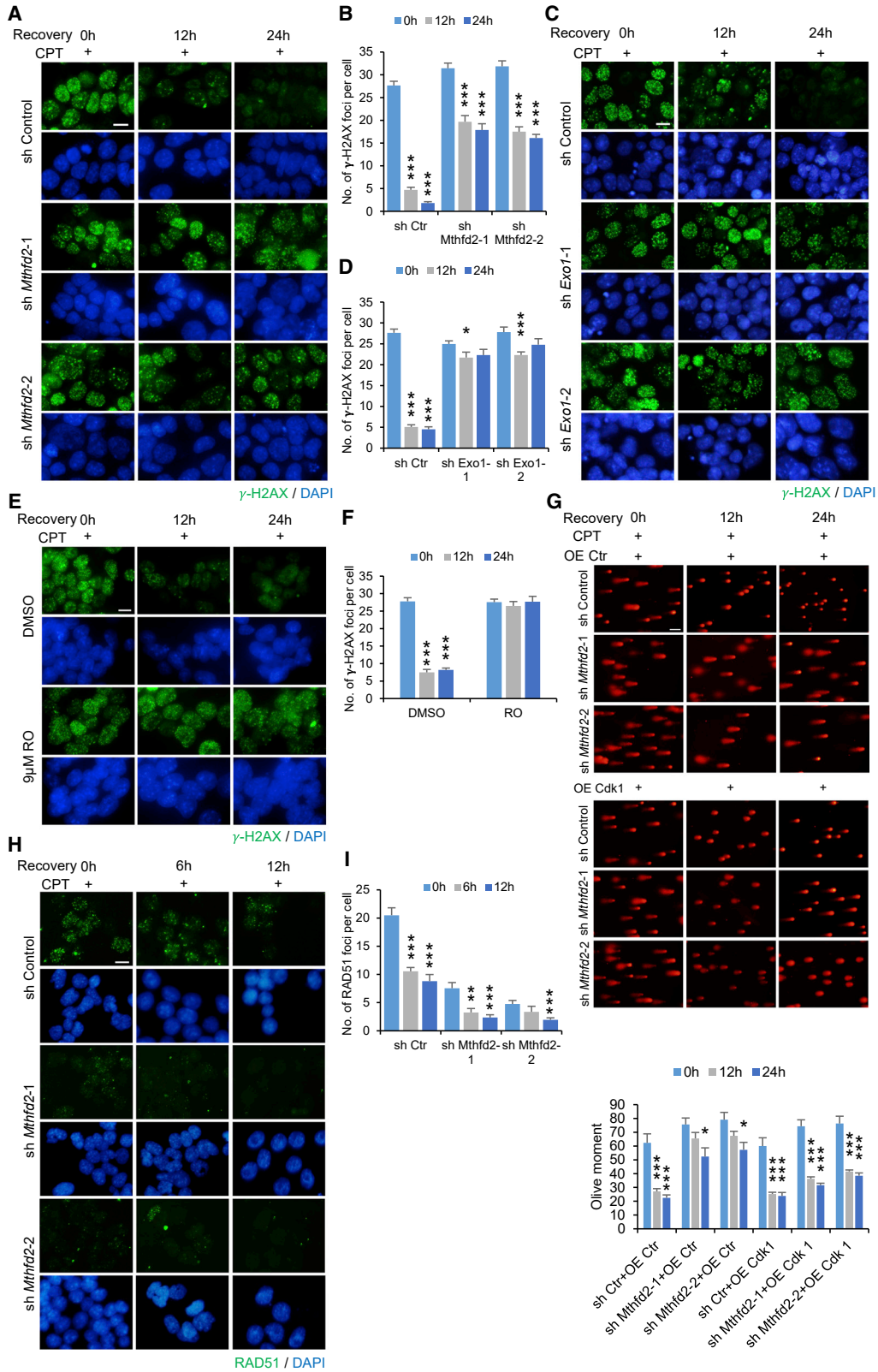## *Mthfd2* Regulates Pluripotency of PSCs by Mediating Both Mitochondrial Function and HR Repair

To further confirm whether *Mthfd2* regulates pluripotency of PSCs by mediating both mitochondrial function and HR repair, on the one hand we transfected mESCs with two sets of shRNAs against *Uqcrc2* or *Exo1*. Depletion of *Uqcrc2* or *Exo1* led to the differentiation of mESCs (Figures S7A–S7G). Moreover, cosuppression of *Uqcrc2* and *Exo1* led to the differentiation of mESCs with reduced AP staining (Figures 7A and 7B), and the expression pattern of marker genes in these cells was more consistent with that in

---

(F and G) GST pull-down assays for interaction between EXO1-His (F), CDK1-His (G), and MTHFD2-GST fusion proteins at 250 mM NaCl containing GST binding buffer.

(H) Representative results showing the EXO1 phosphorylation status in *Mthfd2* KD mESCs.

Data in (A) to (C) are pooled from three independent experiments (mean ± SEM). *p < 0.05, **p < 0.01, ***p < 0.001 (Student's t test) compared with the control. See also Figure S6.

γ-H2AX / DAPI

γ-H2AX / DAPI

γ-H2AX / DAPI

RAD51 / DAPI

(legend on next page)

Mthfd2 KD mESCs (Figures 7C and 7D). On the other hand, we forced the expression either of *Uqcrc2* or *Cdk1* alone or of *Uqcrc2* and *Cdk1* together in *Mthfd2* KD mESCs (Figures 7E and 7F). Forced co-expression of *Uqcrc2* and *Cdk1* rescued the *Mthfd2* KD-induced changes in cell morphology (Figure 7E) and marker gene expression (Figures 7G and 7H), highlighting that *Mthfd2* regulates pluripotency of PSCs by mediating both mitochondrial function and HR repair.

DISCUSSION

High-quality PSCs can differentiate into various types of cells more stably and efficiently, ensuring application security. Many cellular processes, such as pluripotent gene transcription, epigenetic modification, metabolic remodeling, and genomic integrity were involved in somatic cell reprogramming and cell-fate determination (Doege et al., 2012; Graf et al., 2017; Mathieu and Ruohola-Baker, 2017; Silva et al., 2009), but the mechanisms determining the quality of PSCs remain unclear. In our study, we performed transcriptome analysis combined with an IP-MS assay to reveal that *Mthfd2* regulates both mitochondrial function and HR repair and that *Mthfd2* is a powerful bifunctional regulator for quality of PSCs.

We found that mESCs with inhibited MTHFD2 enzymatic activity retained typical stem cell characteristics. Moreover, the expression of key genes in folate metabolism did not differ between *Mthfd2* KD mESCs and control mESCs (Table S2). These results revealed that *Mthfd2* has non-enzymatic functions in mESCs. *MTHFD2* depletion resulted in an obvious suppression of proliferation and cell death in diverse cancer cell types (Nilsson et al., 2014). In our study, homozygous *Mthfd2* KO mESCs showed compromised proliferation, but there was no significant change in cell proliferation in *Mthfd2* KD mESCs (Table S7). Whether this difference was due to residual MTHFD2

activity in *Mthfd2* KD cells, the activity of other enzymes such as MTHFD2L, or the presence of alternative metabolic pathways that are active in mESCs, is unclear. *MTHFD2* depletion resulted in increased glycolysis in breast cancer cells and lung cancer cells (Koufaris et al., 2016; Nishimura et al., 2019). Our results showed that *Mthfd2* KD induces mitochondrial dysfunction, which suggests that in *Mthfd2*-depleted cells mitochondrial dysfunction may force cells to rely mainly on glycolysis to support the cellular ATP demand. However, we cannot rule out the possibility that increased glycolysis is related to mESC differentiation.

Numerous metabolic enzymes, which are often highly expressed by embryonic or undifferentiated cell types, have previously been found to have non-enzymatic functions in the nucleus (Lincet and Icard, 2015). In mESCs, we identified a role of nuclear *Mthfd2* in preserving HR repair. FILIA physically interacts with PARP1 and stimulates PARP1's enzymatic activity to regulate the DDR (Zhao et al., 2015). Our study indicated that *Mthfd2* plays a role similar to that of *Filia* in the DDR. MTHFD2 directly interacts with CDK1 and affects CDK1's activity to regulate EXO1 phosphorylation, thereby promoting HR repair. The most dangerous form of DNA damage is DSBs that can arise from ROS and others. *Mthfd2* overexpression in the *Drosophila* abdominal fat body significantly reduced ROS levels (Yu et al., 2015), and ROS levels were increased in *Mthfd2* KD mESCs. Hence, *Mthfd2* can maintain genomic integrity by both reducing the levels of ROS and promoting HR repair. Genomic stability is necessary for the survival and function of PSCs (Blanpain et al., 2011) and is also a key aspect of improving the quality of iPSCs (Gonzalez et al., 2013; Jiang et al., 2013). Therefore, *Mthfd2* improves the quality of iPSCs by maintaining genomic stability, thereby ensuring the safety of iPSC applications.

Metabolic transition from OXPHOS to glycolysis is a necessary process for successful reprogramming (Folmes

Figure 6. *Mthfd2* **Modulates HR Repair by Regulating EXO1 Phosphorylation**
(A and B) IF staining for γ-H2AX in *Mthfd2* KD mESCs at indicated times post CPT treatment. Representative images (A) and quantification of the average number of γ-H2AX foci per cell (B) (n = 50 nuclei) are shown. DAPI was used to indicate the nuclei. Scale bar, 50 μm.
(C and D) IF staining for γ-H2AX in *Exo1* KD mESCs at indicated times post CPT treatment. Representative images (C) and quantification of the average number of γ-H2AX foci per cell (D) (n = 50 nuclei) are shown. DAPI was used to indicate the nuclei. Scale bar, 50 μm.
(E and F) Immunofluorescence staining for γ-H2AX in RO-3306 (RO)-treated mESCs at indicated times post CPT treatment. Representative images (E) and quantification of the average number of γ-H2AX foci per cell (F) (n = 50 nuclei) are shown. DAPI was used to indicate the nuclei. Scale bar, 50 μm.
(G) DNA damage levels in OE *Cdk1-Mthfd2* KD mESCs were evaluated by the comet assay at indicated times post CPT treatment. Representative images (upper panels) and quantification of the mean olive tail moment (lower panel) (n = 50 nuclei) are shown. Scale bar, 100 μm.
(H and I) IF staining for RAD51 in *Mthfd2* KD mESCs at indicated times post CPT treatment. Representative images (H) and quantification of the average number of Rad51 foci per cell (I) (n = 50 nuclei) are shown. DAPI was used to indicate the nuclei. Scale bar, 20 μm.
All data are pooled from three independent experiments (mean ± SEM). *p < 0.05, **p < 0.01, ***p < 0.001 (Student's t test) compared with the control. See also Figure S6.
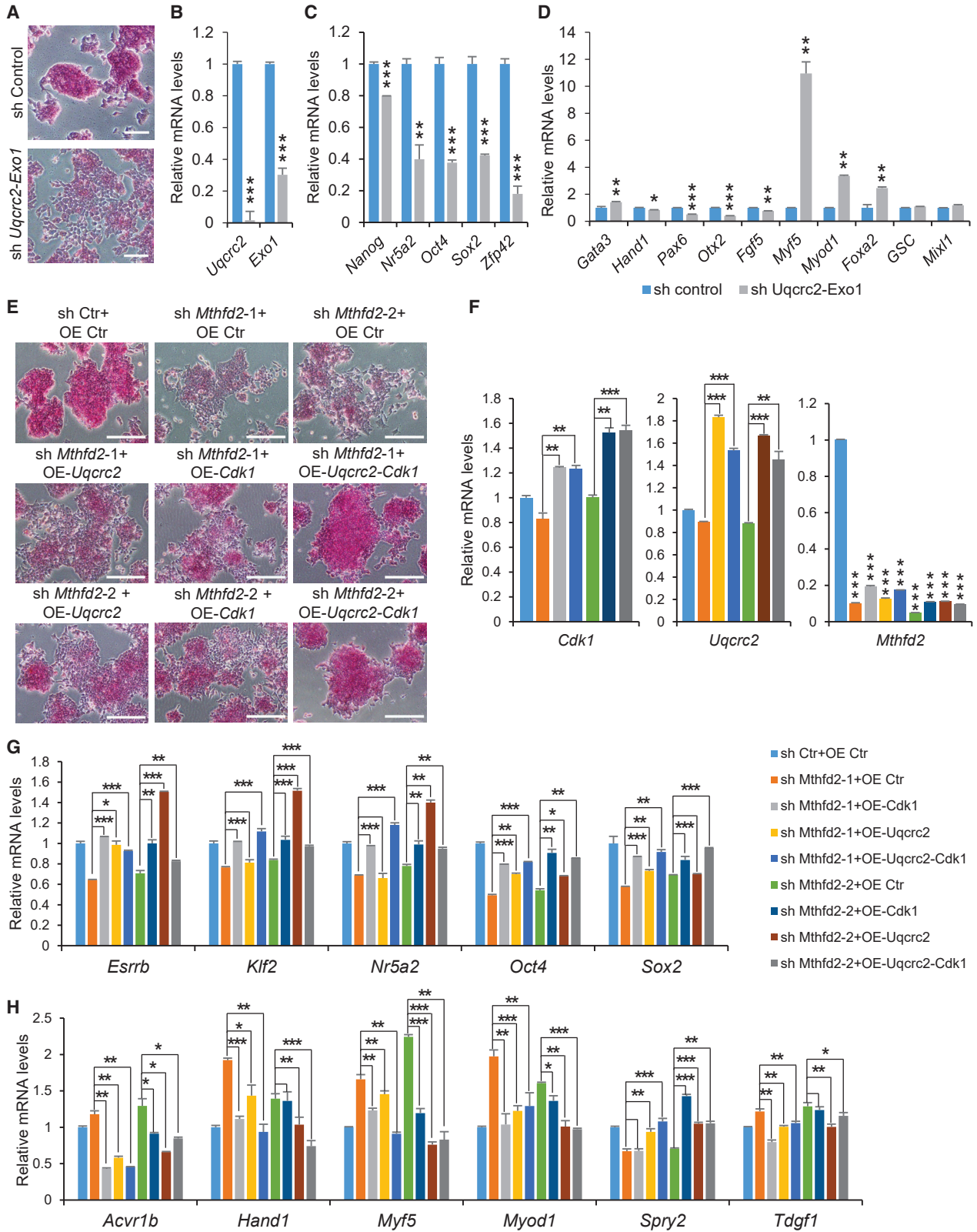
(legend on next page)

et al., 2011; Prigione et al., 2014). However, OXPHOS is also induced and activated at different stages of reprogramming to jointly promote reprogramming (Hawkins et al., 2016; Kida et al., 2015). In our study, overexpression of *Mthfd2* facilitated iPSC induction, suggesting that maintaining active mitochondrial function during reprogramming is beneficial for improving reprogramming efficiency. In PSCs, the metabolic transition from glycolysis to OXPHOS promotes the primed-to-naive state transition (Carbognin et al., 2016). Therefore, in addition to maintaining genomic stability, *Mthfd2* also improves the quality of PSCs by maintaining active OXPHOS. Primed PSCs have lower mitochondrial respiration rates than naive PSCs, which is attributable to a deficiency in ETC complex IV (Zhou et al., 2012). We found that deficiency in ETC complex III also affects the pluripotency state of mESCs. Complex III has two sites, Qo and Qi, to produce ROS. Antimycin A inhibits complex III at the Qi site and increases ROS generation from the Qo site, while it inhibits the Qo site and reduces ROS production (Chen et al., 2003; Demin et al., 1998; Muller et al., 2002). Therefore, *Mthfd2* or *Uqcrc2* depletion may lead to increased ROS production by inhibiting the Qi site instead of the Qo site. MTHFD2 interacts with UQCRC2 to maintain active mitochondrial function, but the interaction is not direct and is mediated by other factors that need further study.

Finally, *Mthfd2* was highly expressed in high-quality iPSCs, and OSKM2 iPSCs were able to develop into viable offspring via tetraploid complementation. The tetraploid complementation assay is the most stringent criterion for assessing the developmental potential of non-human PSCs. Therefore, establishing a fast and effective method to evaluate the pluripotent state of human PSCs is necessary. Moreover, the PSCs of domestic animals such as porcine, bovine, and ovine are still unable to produce chimeras. MTHFD2 is a highly conserved protein between mice and human or domestic animals. Hence, our study should provide new insights into cell pluripotency of other species and provide additional methods to enhance and optimize the acquisition and maintenance of high-quality PSCs.

EXPERIMENTAL PROCEDURES

Co-immunoprecipitation

Cell extracts were prepared in lysis buffer (Beyotime) supplemented with protease inhibitor cocktail and phosphatase inhibitor cocktail (Cell Signaling Technology). To reduce the background, we cleaned the cell extracts with mouse or rabbit immunoglobulin G beads before conducting coIP assays. Antibodies were incubated overnight with cell extracts and then bound to Protein-G beads (Roche) following the manufacturer's protocol. Beads were washed extensively in lysis buffer and then boiled in 2× SDS loading buffer before western blotting.

Data and Code Availability

The accession numbers for the RNA-seq data reported in this paper is SRA: SRP149554.

SUPPLEMENTAL INFORMATION

Supplemental Information can be found online at https://doi.org/10.1016/j.stemcr.2020.06.018.

AUTHOR CONTRIBUTIONS

ACKNOWLEDGMENTS

Figure 7. *Mthfd2* Regulates Pluripotency of mESCs by Modulating both Mitochondrial Function and DNA Repair
(A) Representative results of *Uqcrc2-Exo1* KD mESCs with AP staining. Scale bars, 100 μm.
(B) qRT-PCR analysis of mRNA levels of *Uqcrc2* and *Exo1* in *Uqcrc2-Exo1* KD mESCs.
(C and D) qRT-PCR analysis of mRNA levels of pluripotency marker genes (C) and lineage marker genes (D) in *Uqcrc2-Exo1* KD mESCs.
(E) Representative results of OE *Uqcrc2*-, OE *Cdk1*- or co-OE *Uqcrc2*, and *Cdk1-Mthfd2* KD mESCs with AP staining. Scale bars, 200 μm.
(F) qRT-PCR analysis of mRNA levels of *Uqcrc2*, *Cdk1*, and *Mthfd2* in OE *Uqcrc2*-, OE *Cdk1*- or co-OE *Uqcrc2*, and *Cdk1-Mthfd2* KD mESCs.
(G and H) qRT-PCR analysis of mRNA levels of pluripotency marker genes (G) and lineage marker genes (H) in OE *Uqcrc2*-, OE *Cdk1*- or co-OE *Uqcrc2*, and *Cdk1-Mthfd2* KD mESCs.
Data in (B) to (D) and (F) to (H) are pooled from three independent experiments (mean ± SD) relative to EF1-α and the control. *$p < 0.05$, **$p < 0.01$, ***$p < 0.001$ (Student's t test) compared with the control. See also Figure S7.

REFERENCES

Aguilera-Aguirre, L., Bacsi, A., Saavedra-Molina, A., Kurosky, A., Sur, S., and Boldogh, I. (2009). Mitochondrial dysfunction increases allergic airway inflammation. J. Immunol. *183*, 5379–5387.

Asai, A., Koseki, J., Konno, M., Nishimura, T., Gotoh, N., Satoh, T., Doki, Y., Mori, M., and Ishii, H. (2018). Drug discovery of anticancer drugs targeting methylenetetrahydrofolate dehydrogenase 2. Heliyon *4*, e01021.

Blanpain, C., Mohrin, M., Sotiropoulou, P.A., and Passegue, E. (2011). DNA-damage response in tissue-specific and cancer stem cells. Cell Stem Cell *8*, 16–29.

Boroviak, T., Loos, R., Lombard, P., Okahara, J., Behr, R., Sasaki, E., Nichols, J., Smith, A., and Bertone, P. (2015). Lineage-specific profiling delineates the emergence and progression of naive pluripotency in mammalian embryogenesis. Dev. Cell *35*, 366–382.

Carbognin, E., Betto, R.M., Soriano, M.E., Smith, A.G., and Martello, G. (2016). Stat3 promotes mitochondrial transcription and oxidative respiration during maintenance and induction of naive pluripotency. EMBO J. *35*, 618–634.

Chen, K., Long, Q., Wang, T., Zhao, D., Zhou, Y., Qi, J., Wu, Y., Li, S., Chen, C., Zeng, X., et al. (2016). Gadd45a is a heterochromatin relaxer that enhances iPS cell generation. EMBO Rep. *17*, 1641–1656.

Chen, Q., Vazquez, E.J., Moghaddas, S., Hoppel, C.L., and Lesnefsky, E.J. (2003). Production of reactive oxygen species by mitochondria: central role of complex III. J. Biol. Chem. *278*, 36027–36031.

Crofts, A.R. (2004). The cytochrome bc1 complex: function in the context of structure. Annu. Rev. Physiol. *66*, 689–733.

Demin, O.V., Kholodenko, B.N., and Skulachev, V.P. (1998). A model of O2.-generation in the complex III of the electron transport chain. Mol. Cell. Biochem. *184*, 21–33.

Desmarais, J.A., Unger, C., Damjanov, I., Meuth, M., and Andrews, P. (2016). Apoptosis and failure of checkpoint kinase 1 activation in human induced pluripotent stem cells under replication stress. Stem Cell Res. Ther. *7*, 17.

Di Pietro, E., Sirois, J., Tremblay, M.L., and MacKenzie, R.E. (2002). Mitochondrial NAD-dependent methylenetetrahydrofolate dehydrogenase-methenyltetrahydrofolate cyclohydrolase is essential for embryonic development. Mol. Cell. Biol. *22*, 4158–4166.

Doege, C.A., Inoue, K., Yamashita, T., Rhee, D.B., Travis, S., Fujita, R., Guarnieri, P., Bhagat, G., Vanti, W.B., Shih, A., et al. (2012). Early-stage epigenetic modification during somatic cell reprogramming by Parp1 and Tet2. Nature *488*, 652–655.

Evans, M.J., and Kaufman, M.H. (1981). Establishment in culture of pluripotential cells from mouse embryos. Nature *292*, 154–156.

Feng, B., Jiang, J., Kraus, P., Ng, J.-H., Heng, J.-C.D., Chan, Y.-S., Yaw, L.-P., Zhang, W., Loh, Y.-H., Han, J., et al. (2009). Reprogramming of fibroblasts into induced pluripotent stem cells with orphan nuclear receptor Esrrb. Nat. Cell Biol. *11*, 197–203.

Folmes, C.D., Nelson, T.J., Martinez-Fernandez, A., Arrell, D.K., Lindor, J.Z., Dzeja, P.P., Ikeda, Y., Perez-Terzic, C., and Terzic, A. (2011). Somatic oxidative bioenergetics transitions into pluripotency-dependent glycolysis to facilitate nuclear reprogramming. Cell Metab. *14*, 264–271.

Gao, S., Wang, Z.L., Di, K.Q., Chang, G., Tao, L., An, L., Wu, F.J., Xu, J.Q., Liu, Y.W., Wu, Z.H., et al. (2013). Melatonin improves the reprogramming efficiency of murine-induced pluripotent stem cells using a secondary inducible system. J. Pineal Res. *55*, 31–39.

Gonzalez, F., Georgieva, D., Vanoli, F., Shi, Z.D., Stadtfeld, M., Ludwig, T., Jasin, M., and Huangfu, D. (2013). Homologous recombination DNA repair genes play a critical role in reprogramming to a pluripotent state. Cell Rep. *3*, 651–660.

Graf, U., Casanova, E.A., Wyck, S., Dalcher, D., Gatti, M., Vollenweider, E., Okoniewski, M.J., Weber, F.A., Patel, S.S., Schmid, M.W., et al. (2017). Pramel7 mediates ground-state pluripotency through proteasomal-epigenetic combined pathways. Nat. Cell Biol. *19*, 763–773.

Gustafsson Sheppard, N., Jarl, L., Mahadessian, D., Strittmatter, L., Schmidt, A., Madhusudan, N., Tegner, J., Lundberg, E.K., Asplund, A., Jain, M., et al. (2015). The folate-coupled enzyme MTHFD2 is a nuclear protein and promotes cell proliferation. Sci. Rep. *5*, 15029.

Han, J., Yuan, P., Yang, H., Zhang, J., Soh, B.S., Li, P., Lim, S.L., Cao, S., Tay, J., Orlov, Y.L., et al. (2010). Tbx3 improves the germ-line competency of induced pluripotent stem cells. Nature *463*, 1096–1100.

Hatefi, Y. (1985). The mitochondrial electron transport and oxidative phosphorylation system. Annu. Rev. Biochem. *54*, 1015–1069.

Hawkins, K.E., Joy, S., Delhove, J.M., Kotiadis, V.N., Fernandez, E., Fitzpatrick, L.M., Whiteford, J.R., King, P.J., Bolanos, J.P., Duchen, M.R., et al. (2016). NRF2 orchestrates the metabolic shift during induced pluripotent stem cell reprogramming. Cell Rep. *14*, 1883–1891.

Heng, J.C., Feng, B., Han, J., Jiang, J., Kraus, P., Ng, J.H., Orlov, Y.L., Huss, M., Yang, L., Lufkin, T., et al. (2010). The nuclear receptor Nr5a2 can replace Oct4 in the reprogramming of murine somatic cells to pluripotent cells. Cell Stem Cell *6*, 167–174.

Hsiang, Y.H., Lihou, M.G., and Liu, L.F. (1989). Arrest of replication forks by drug-stabilized topoisomerase I-DNA cleavable complexes as a mechanism of cell killing by camptothecin. Cancer Res. *49*, 5077–5082.

Huang, Y., Osorno, R., Tsakiridis, A., and Wilson, V. (2012). In vivo differentiation potential of epiblast stem cells revealed by chimeric embryo formation. Cell Rep. *2*, 1571–1578.

Jackson, S.P. (2002). Sensing and repairing DNA double-strand breaks. Carcinogenesis *23*, 687–696.

Jiang, J., Lv, W., Ye, X., Wang, L., Zhang, M., Yang, H., Okuka, M., Zhou, C., Zhang, X., Liu, L., et al. (2013). Zscan4 promotes genomic stability during reprogramming and dramatically improves the quality of iPS cells as demonstrated by tetraploid complementation. Cell Res. *23*, 92–106.

Khacho, M., Clark, A., Svoboda, D.S., Azzi, J., MacLaurin, J.G., Meghaizel, C., Sesaki, H., Lagace, D.C., Germain, M., Harper, M.E., et al. (2016). Mitochondrial dynamics impacts stem cell identity and fate decisions by regulating a nuclear transcriptional Program. Cell Stem Cell 19, 232–247.

Kida, Y.S., Kawamura, T., Wei, Z., Sogo, T., Jacinto, S., Shigeno, A., Kushige, H., Yoshihara, E., Liddle, C., Ecker, J.R., et al. (2015). ERRs mediate a metabolic switch required for somatic cell reprogramming to pluripotency. Cell Stem Cell 16, 547–555.

Koufaris, C., Gallage, S., Yang, T., Lau, C.H., Valbuena, G.N., and Keun, H.C. (2016). Suppression of MTHFD2 in MCF-7 breast cancer cells increases glycolysis, dependency on exogenous Glycine, and sensitivity to folate depletion. J. Proteome Res. 15, 2618–2625.

Lee, J.Y., Kim, D.K., Ko, J.J., Kim, K.P., and Park, K.S. (2016). Rad51 regulates reprogramming efficiency through DNA repair pathway. Dev. Reprod. 20, 163–169.

Li, M., He, Y., Dubois, W., Wu, X., Shi, J., and Huang, J. (2012). Distinct regulatory mechanisms and functions for p53-activated and p53-repressed DNA damage response genes in embryonic stem cells. Mol. Cell 46, 30–42.

Lin, H., Huang, B., Wang, H., Liu, X., Hong, Y., Qiu, S., and Zheng, J. (2018). MTHFD2 overexpression predicts poor prognosis in renal cell carcinoma and is associated with cell proliferation and vimentin-modulated migration and invasion. Cell. Physiol. Biochem. 51, 991–1000.

Lin, T., Chao, C., Saito, S., Mazur, S.J., Murphy, M.E., Appella, E., and Xu, Y. (2005). p53 induces differentiation of mouse embryonic stem cells by suppressing Nanog expression. Nat. Cell Biol. 7, 165–171.

Lincet, H., and Icard, P. (2015). How do glycolytic enzymes favour cancer cell proliferation by nonmetabolic functions? Oncogene 34, 3751–3759.

Liu, F., Liu, Y., He, C., Tao, L., He, X., Song, H., and Zhang, G. (2014a). Increased MTHFD2 expression is associated with poor prognosis in breast cancer. Tumour Biol. 35, 8685–8690.

Liu, J.C., Guan, X., Ryan, J.A., Rivera, A.G., Mock, C., Agrawal, V., Letai, A., Lerou, P.H., and Lahav, G. (2013). High mitochondrial priming sensitizes hESCs to DNA-damage-induced apoptosis. Cell Stem Cell 13, 483–491.

Liu, K., Wang, F., Ye, X., Wang, L., Yang, J., Zhang, J., and Liu, L. (2014b). KSR-based medium improves the generation of high-quality mouse iPS cells. PLoS One 9, e105309.

Mathieu, J., and Ruohola-Baker, H. (2017). Metabolic remodeling during the loss and acquisition of pluripotency. Development 144, 541–551.

Mitchell, P. (1975). Protonmotive redox mechanism of the cytochrome b-c1 complex in the respiratory chain: protonmotive ubiquinone cycle. FEBS Lett. 56, 1–6.

Miyake, N., Yano, S., Sakai, C., Hatakeyama, H., Matsushima, Y., Shiina, M., Watanabe, Y., Bartley, J., Abdenur, J.E., Wang, R.Y., et al. (2013). Mitochondrial complex III deficiency caused by a homozygous UQCRC2 mutation presenting with neonatal-onset recurrent metabolic decompensation. Hum. Mutat. 34, 446–452.

Muller, F., Crofts, A.R., and Kramer, D.M. (2002). Multiple Q-cycle bypass reactions at the Qo site of the cytochrome bc1 complex. Biochemistry 41, 7866–7874.

Nichols, J., and Smith, A. (2009). Naive and primed pluripotent states. Cell Stem Cell 4, 487–492.

Nilsson, R., Jain, M., Madhusudhan, N., Sheppard, N.G., Strittmatter, L., Kampf, C., Huang, J., Asplund, A., and Mootha, V.K. (2014). Metabolic enzyme expression highlights a key role for MTHFD2 and the mitochondrial folate pathway in cancer. Nat. Commun. 5, 3128.

Nishimura, T., Nakata, A., Chen, X., Nishi, K., Meguro-Horike, M., Sasaki, S., Kita, K., Horike, S.I., Saitoh, K., Kato, K., et al. (2019). Cancer stem-like properties and gefitinib resistance are dependent on purine synthetic metabolism mediated by the mitochondrial enzyme MTHFD2. Oncogene 38, 2464–2481.

Pei, Y., Yue, L., Zhang, W., Wang, Y., Wen, B., Zhong, L., Xiang, J., Li, J., Zhang, S., Wang, H., et al. (2015). Improvement in mouse iPSC induction by Rab32 reveals the importance of lipid metabolism during reprogramming. Sci. Rep. 5, 16539.

Pikman, Y., Puissant, A., Alexe, G., Furman, A., Chen, L.M., Frumm, S.M., Ross, L., Fenouille, N., Bassil, C.F., Lewis, C.A., et al. (2016). Targeting MTHFD2 in acute myeloid leukemia. J. Exp. Med. 213, 1285–1306.

Prigione, A., Rohwer, N., Hoffmann, S., Mlody, B., Drews, K., Bukowiecki, R., Blumlein, K., Wanker, E.E., Ralser, M., Cramer, T., et al. (2014). HIF1alpha modulates cell fate reprogramming through early glycolytic shift and upregulation of PDK1-3 and PKM2. Stem Cells 32, 364–376.

Rogakou, E.P., Pilch, D.R., Orr, A.H., Ivanova, V.S., and Bonner, W.M. (1998). DNA double-stranded breaks induce histone H2AX phosphorylation on serine 139. J. Biol. Chem. 273, 5858–5868.

Ryu, J.M., Lee, H.J., Jung, Y.H., Lee, K.H., Kim, D.I., Kim, J.Y., Ko, S.H., Choi, G.E., Chai, , II, Song, E.J., et al. (2015). Regulation of stem cell fate by ROS-mediated alteration of metabolism. Int. J. Stem Cells 8, 24–35.

Schaetzlein, S., Kodandaramireddy, N.R., Ju, Z., Lechel, A., Stepczynska, A., Lilli, D.R., Clark, A.B., Rudolph, C., Kuhnel, F., Wei, K., et al. (2007). Exonuclease-1 deletion impairs DNA damage signaling and prolongs lifespan of telomere-dysfunctional mice. Cell 130, 863–877.

Shyh-Chang, N., and Daley, G.Q. (2015). Metabolic switches linked to pluripotency and embryonic stem cell differentiation. Cell Metab. 21, 349–350.

Silva, J., Nichols, J., Theunissen, T.W., Guo, G., van Oosten, A.L., Barrandon, O., Wray, J., Yamanaka, S., Chambers, I., and Smith, A. (2009). Nanog is the gateway to the pluripotent ground state. Cell 138, 722–737.

Sukumar, M., Liu, J., Mehta, G.U., Patel, S.J., Roychoudhuri, R., Crompton, J.G., Klebanoff, C.A., Ji, Y., Li, P., Yu, Z., et al. (2016). Mitochondrial membrane potential identifies cells with enhanced stemness for cellular therapy. Cell Metab. 23, 63–76.

Takahashi, K., and Yamanaka, S. (2006). Induction of pluripotent stem cells from mouse embryonic and adult fibroblast cultures by defined factors. Cell 126, 663–676.

Takashima, Y., Guo, G., Loos, R., Nichols, J., Ficz, G., Krueger, F., Oxley, D., Santos, F., Clarke, J., Mansfield, W., et al. (2014). Resetting transcription factor control circuitry toward ground-state pluripotency in human. Cell 158, 1254–1269.

Tesar, P.J., Chenoweth, J.G., Brook, F.A., Davies, T.J., Evans, E.P., Mack, D.L., Gardner, R.L., and McKay, R.D. (2007). New cell lines from mouse epiblast share defining features with human embryonic stem cells. Nature 448, 196–199.

Tibbetts, A.S., and Appling, D.R. (2010). Compartmentalization of Mammalian folate-mediated one-carbon metabolism. Annu. Rev. Nutr. 30, 57–81.

Tichy, E.D., Pillai, R., Deng, L., Liang, L., Tischfield, J., Schwemberger, S.J., Babcock, G.F., and Stambrook, P.J. (2010). Mouse embryonic stem cells, but not somatic cells, predominantly use homologous recombination to repair double-strand DNA breaks. Stem Cells Dev. 19, 1699–1711.

Tomimatsu, N., Mukherjee, B., Catherine Hardebeck, M., Ilcheva, M., Vanessa Camacho, C., Louise Harris, J., Porteus, M., Llorente, B., Khanna, K.K., and Burma, S. (2014). Phosphorylation of EXO1 by CDKs 1 and 2 regulates DNA end resection and repair pathway choice. Nat. Commun. 5, 3561.

Weissbein, U., Benvenisty, N., and Ben-David, U. (2014). Quality control: genome maintenance in pluripotent stem cells. J. Cell Biol. 204, 153–163.

Xiang, J., Cao, S., Zhong, L., Wang, H., Pei, Y., Wei, Q., Wen, B., Mu, H., Zhang, S., Yue, L., et al. (2018). Pluripotent stem cells secrete Activin A to improve their epiblast competency after injection into recipient embryos. Protein Cell 9, 717–728.

Yoshihara, M., Hayashizaki, Y., and Murakawa, Y. (2017). Genomic instability of iPSCs: challenges towards their clinical applications. Stem Cell Rev. Rep. 13, 7–16.

Yu, S., Jang, Y., Paik, D., Lee, E., and Park, J.J. (2015). Nmdmc overexpression extends Drosophila lifespan and reduces levels of mitochondrial reactive oxygen species. Biochem. Biophys. Res. Commun. 465, 845–850.

Zhang, J., Ratanasirintrawoot, S., Chandrasekaran, S., Wu, Z., Ficarro, S.B., Yu, C., Ross, C.A., Cacchiarelli, D., Xia, Q., Seligson, M., et al. (2016). LIN28 regulates stem cell metabolism and conversion to primed pluripotency. Cell Stem Cell 19, 66–80.

Zhang, J., Tam, W.L., Tong, G.Q., Wu, Q., Chan, H.Y., Soh, B.S., Lou, Y., Yang, J., Ma, Y., Chai, L., et al. (2006). Sall4 modulates embryonic stem cell pluripotency and early embryonic development by the transcriptional regulation of Pou5f1. Nat. Cell Biol. 8, 1114–1123.

Zhang, Y., Cui, P., Li, Y., Feng, G., Tong, M., Guo, L., Li, T., Liu, L., Li, W., and Zhou, Q. (2018). Mitochondrially produced ATP affects stem cell pluripotency via Actl6a-mediated histone acetylation. FASEB J. 32, 1891–1902.

Zhao, B., Zhang, W.D., Duan, Y.L., Lu, Y.Q., Cun, Y.X., Li, C.H., Guo, K., Nie, W.H., Li, L., Zhang, R., et al. (2015). Filia is an ESC-specific regulator of DNA damage response and safeguards genomic stability. Cell Stem Cell 16, 684–698.

Zhao, X.Y., Li, W., Lv, Z., Liu, L., Tong, M., Hai, T., Hao, J., Guo, C.L., Ma, Q.W., Wang, L., et al. (2009). iPS cells produce viable mice through tetraploid complementation. Nature 461, 86–90.

Zhong, X., Cui, P., Cai, Y., Wang, L., He, X., Long, P., Lu, K., Yan, R., Zhang, Y., Pan, X., et al. (2019). Mitochondrial dynamics is critical for the Full pluripotency and embryonic developmental potential of pluripotent stem cells. Cell Metab. 29, 979–992.e4.

Zhou, G., Meng, S., Li, Y., Ghebre, Y.T., and Cooke, J.P. (2016). Optimal ROS signaling is critical for nuclear reprogramming. Cell Rep. 15, 919–925.

Zhou, W., Choi, M., Margineantu, D., Margaretha, L., Hesson, J., Cavanaugh, C., Blau, C.A., Horwitz, M.S., Hockenbery, D., Ware, C., et al. (2012). HIF1alpha induced switch from bivalent to exclusively glycolytic metabolism during ESC-to-EpiSC/hESC transition. EMBO J. 31, 2103–2116.

Supplemental Information

***Mthfd2* Modulates Mitochondrial Function and DNA Repair to Maintain the Pluripotency of Mouse Stem Cells**

Liang Yue, Yangli Pei, Liang Zhong, Henry Yang, Yanliang Wang, Wei Zhang, Naixin Chen, Qianqian Zhu, Jie Gao, Minglei Zhi, Bingqiang Wen, Shaopeng Zhang, Jinzhu Xiang, Qingqing Wei, Hui Liang, Suying Cao, Huiqiang Lou, Zhongzhou Chen, and Jianyong Han

A

B

C

D

E

F

G

H
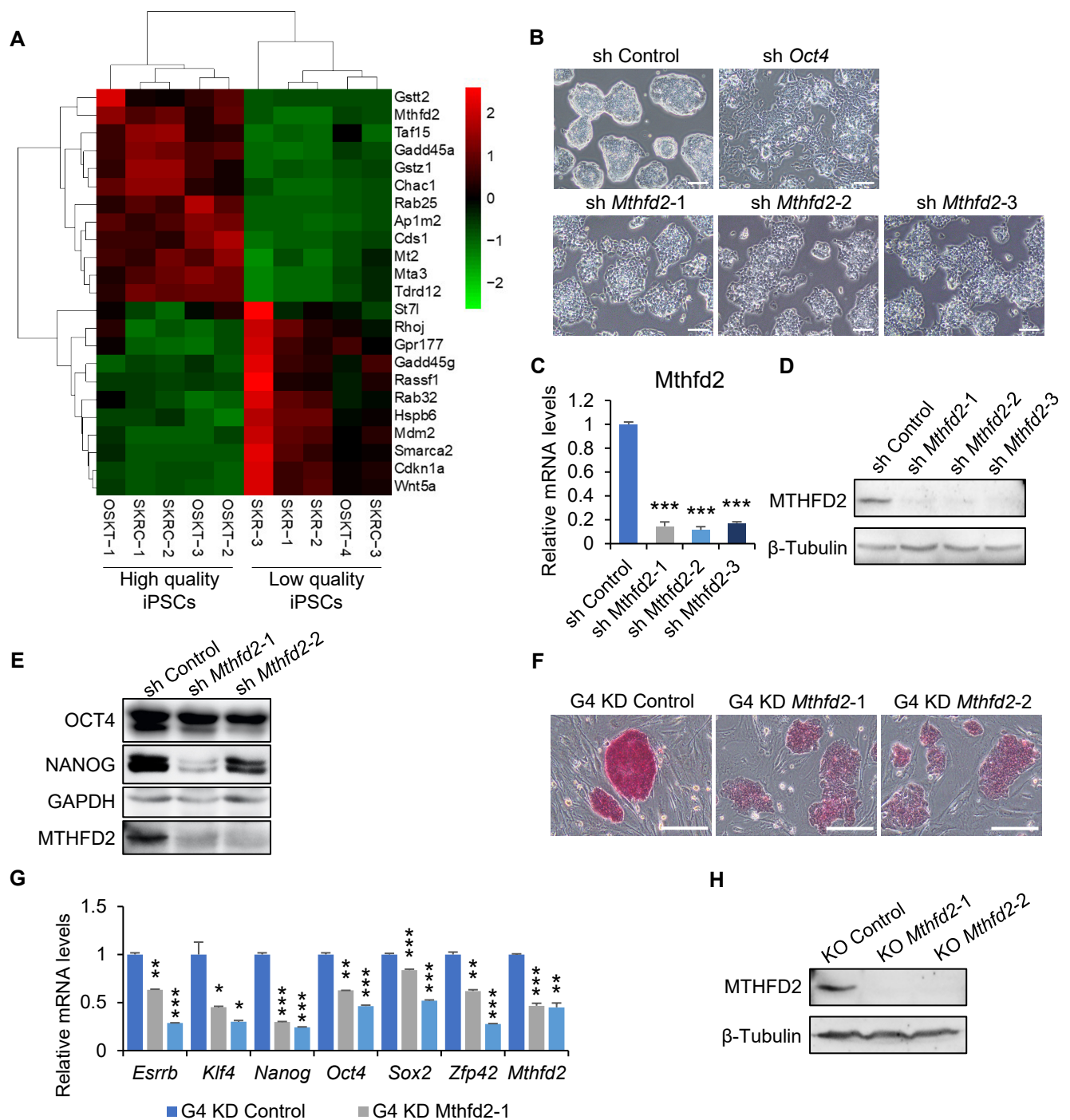
Figure S1. *Mthfd2* **Plays Critical Role in Maintaining Pluripotency in mESCs, Related to Figure 1.**

(A) Heat-map of differentially expressed genes (DEGs) between iPSCs with different pluripotency. For details, see Table S1.

(B) Representative results from shRNAs screen in mESCs. Scale bar, 100 μm. mESCs treated with sh Control was used as negative control, and mESCs treated with sh *Oct4* was used as positive control.

(C) qRT-PCR analysis of mRNA levels of *Mthfd2* in *Mthfd2* KD mESCs.

(D) Western blot (WB) analysis of the level of MTHFD2 protein in *Mthfd2* KD mESCs. β-Tubulin was used as a loading control.

(E) WB analysis of the levels of OCT4 and NANOG protein in *Mthfd2* KD mESCs. GAPDH was used as a loading control.

(F) Representative results of *Mthfd2* KD G4 mESCs with AP staining. Scale bar, 200 μm.

(G) qRT-PCR analysis of mRNA levels of pluripotency marker genes in *Mthfd2* KD G4 mESCs.

(H) WB analysis of the level of MTHFD2 protein in *Mthfd2* KO mESCs. β-Tubulin was used as a loading control.

Data (C and G) are pooled from 3 independent experiments (mean ± SD) relative to EF1-α and the control. *$P < 0.05$, **$P < 0.01$, and ***$P < 0.001$ (Student's t test) compared to the control.
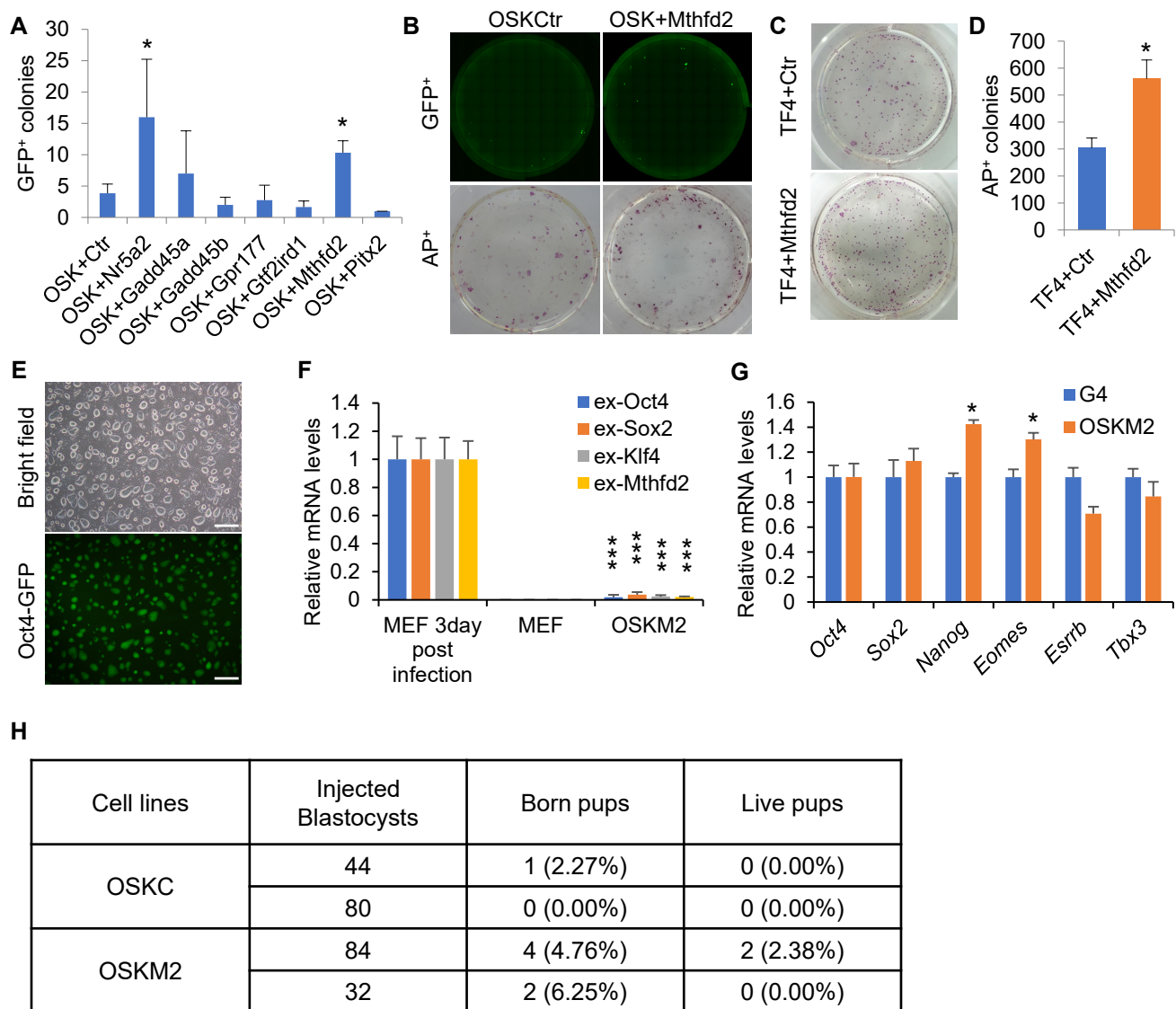
Figure S2. *Mthfd2* Facilitates Mouse iPSC Induction, Related to Figure 2.

(A) The reprogramming efficiencies in mESCs medium. OSK + Control (OSKCtr) cells were used as a control. Data are pooled from 3 independent experiments (mean ± SD). *P < 0.05, **P < 0.01, and ***P < 0.001 (Student's *t* test) compared to the control.

(B) Full-well mosaic images of Oct4-GFP+ cells and AP+ colonies are shown for OSKCtr and OSKM2 iPSCs in mESCs medium.

(C) The reprogramming efficiency was increased by overexpress (OE) Mthfd2 in TF4 MEFs. Data are pooled from 3 independent experiments (mean ± SD). *P < 0.05, **P < 0.01, and ***P < 0.001 (Student's *t* test) compared to the control.

(D) *Mthfd2* OE increases the number of AP+ colonies following the induction of iPSCs in TF4 MEFs. The results from TF4 + Ctr cells were used as a control.

(E) Phase contrast and Oct4-GFP images of iPSC colonies generated by coinfection of *Mthfd2* and OSK. Scale bar, 500 μm.

(F) qRT-PCR analysis of levels of integrated transgenes in OSKM2 iPSCs. Wild type MEFs and three days after retroviral infection of MEFs were used as controls.

(G) qRT-PCR analysis of mRNA levels of pluripotency marker genes in OSKM2 iPSCs. The G4 mESCs was used as controls.

(H) Analysis of the efficiency of live offspring produced by OSKM2 iPSCs and OSKC iPSCs using tetraploid complementation. Data (F and G) are pooled from 3 independent experiments (mean ± SD) relative to EF1-α and the controls. *P < 0.05, **P < 0.01, and ***P < 0.001 (Student's *t* test) compared to the control.
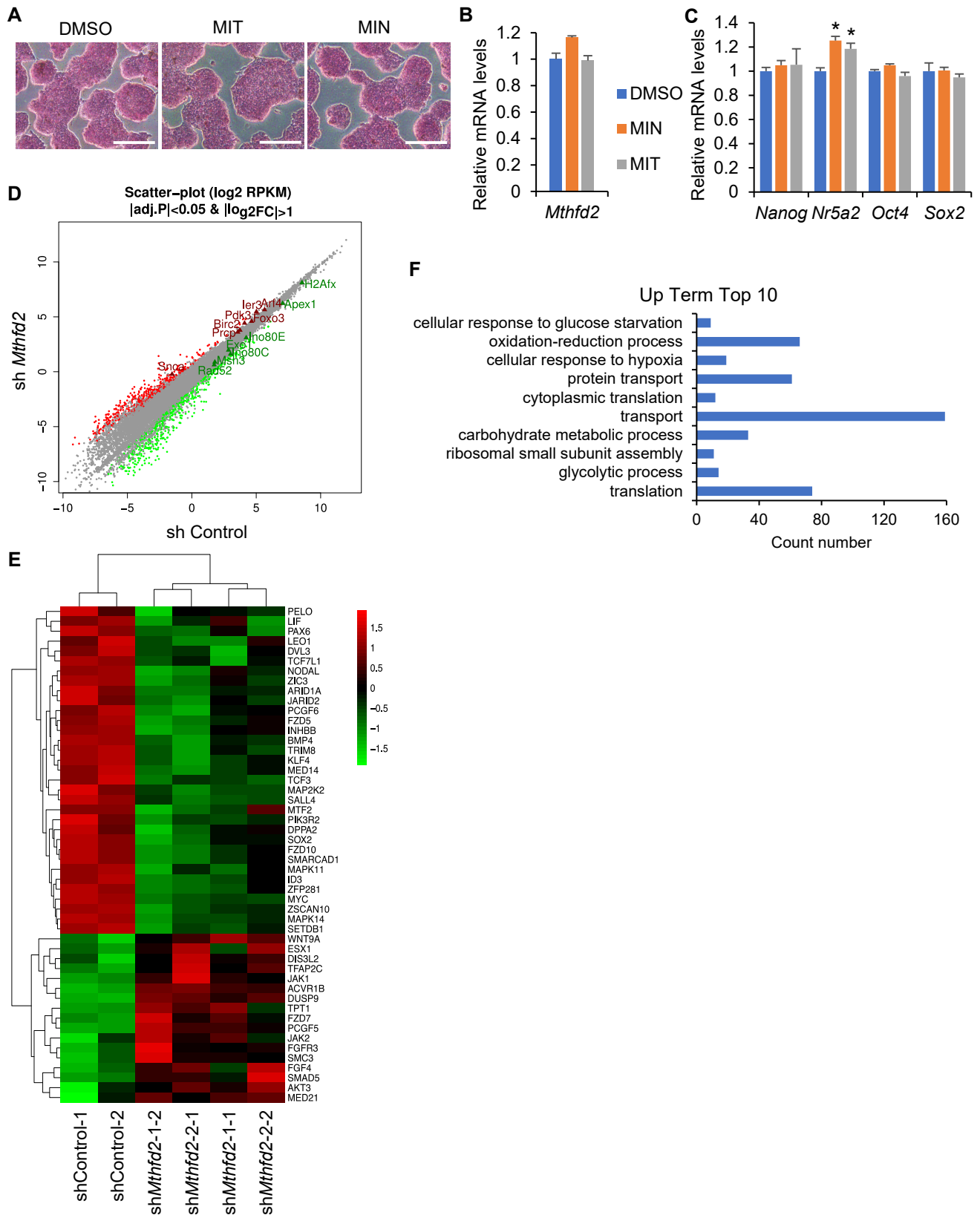
Figure S3. RNA-seq of *Mthfd2* KD mESCs, Related to Figure 3.

(A) Representative results of MI-mESCs with AP staining. Scale bar, 200 μm.

(B and C) qRT-PCR analysis of mRNA levels of *Mthfd2(B)* and pluripotency marker genes (C) in MI-mESCs. Data are pooled from 3 independent experiments (mean ± SD) relative to EF1-α and the control. *$P < 0.05$, **$P < 0.01$, and ***$P < 0.001$ (Student's *t* test) compared to the control.

(D) Scatter plot of DEGs analysis based on RNA-seq data. Two biological replicates were used for both Control mESCs and two sets of *Mthfd2* KD mESCs. See Table S2 for details.

(E) Heat-map of DEGs about pluripotency between Control mESCs and *Mthfd2* KD mESCs.

(F) Top 10 of enriched Gene Ontology (GO) terms potently upregulated by *Mthfd2*.
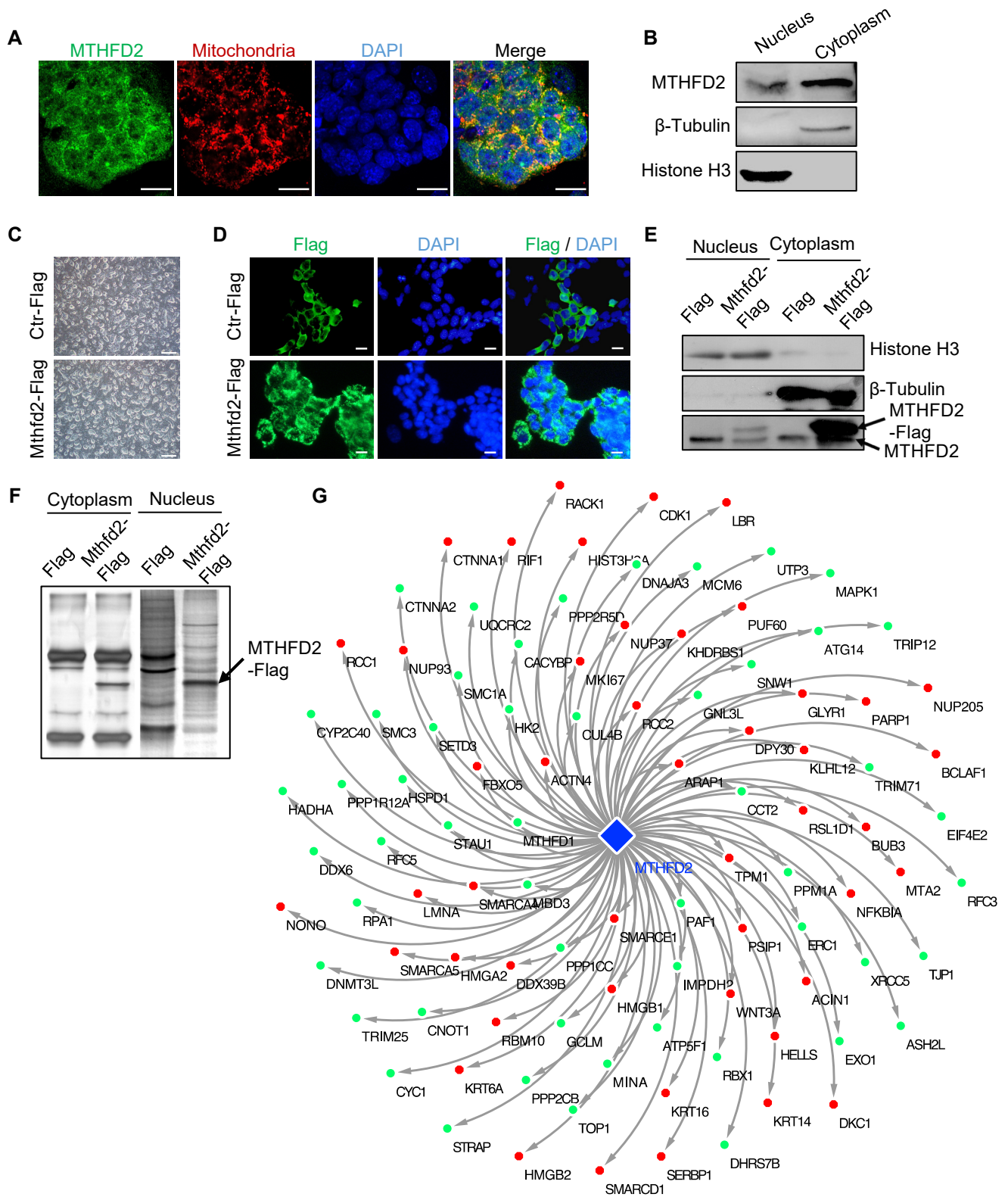
Figure S4. Results of MTHFD2 Interactome Assay, Related to Figure 3.

(A) IF staining for MTHFD2 in the mitochondria and nucleus in mESCs. DAPI was used to indicate the nuclei. Scale bar, 20 μm.

(B) WB analysis of the distribution of the Mthfd2 protein in the cytoplasm and nucleus of mESCs. β-Tubulin and Histone H3 were used as loading controls for the cytoplasmic and nuclear proteins, respectively.

(C) Representative results of Mthfd2-Flag mESCs and control cells (Ctr-Flag). Scale bar, 500 μm.

(D) IF staining for FLAG in Mthfd2-Flag mESCs and Ctr-Flag mESCs. DAPI was used to indicate the nuclei. Scale bar, 20 μm.

(E) WB analysis of the distribution of the MTHFD2 protein in the cytoplasm and nucleus of Mthfd2-Flag mESCs and Ctr-Flag mESCs. β-Tubulin and Histone H3 were used as loading controls for the cytoplasmic and nuclear proteins, respectively.

(F) Cell lysates from Mthfd2-Flag mESCs and Ctr-Flag mESCs were immunoprecipitated with an anti-FLAG antibody. The bound proteins were eluted and resolved by SDS–PAGE and then visualized by silver staining.

(G) Schematic network showing part of the MTHFD2-interacting proteins in mESCs. Red nodes indicate target genes detected in nuclear, green nodes indicate target genes detected in cytoplasm. See Table S3 for details.
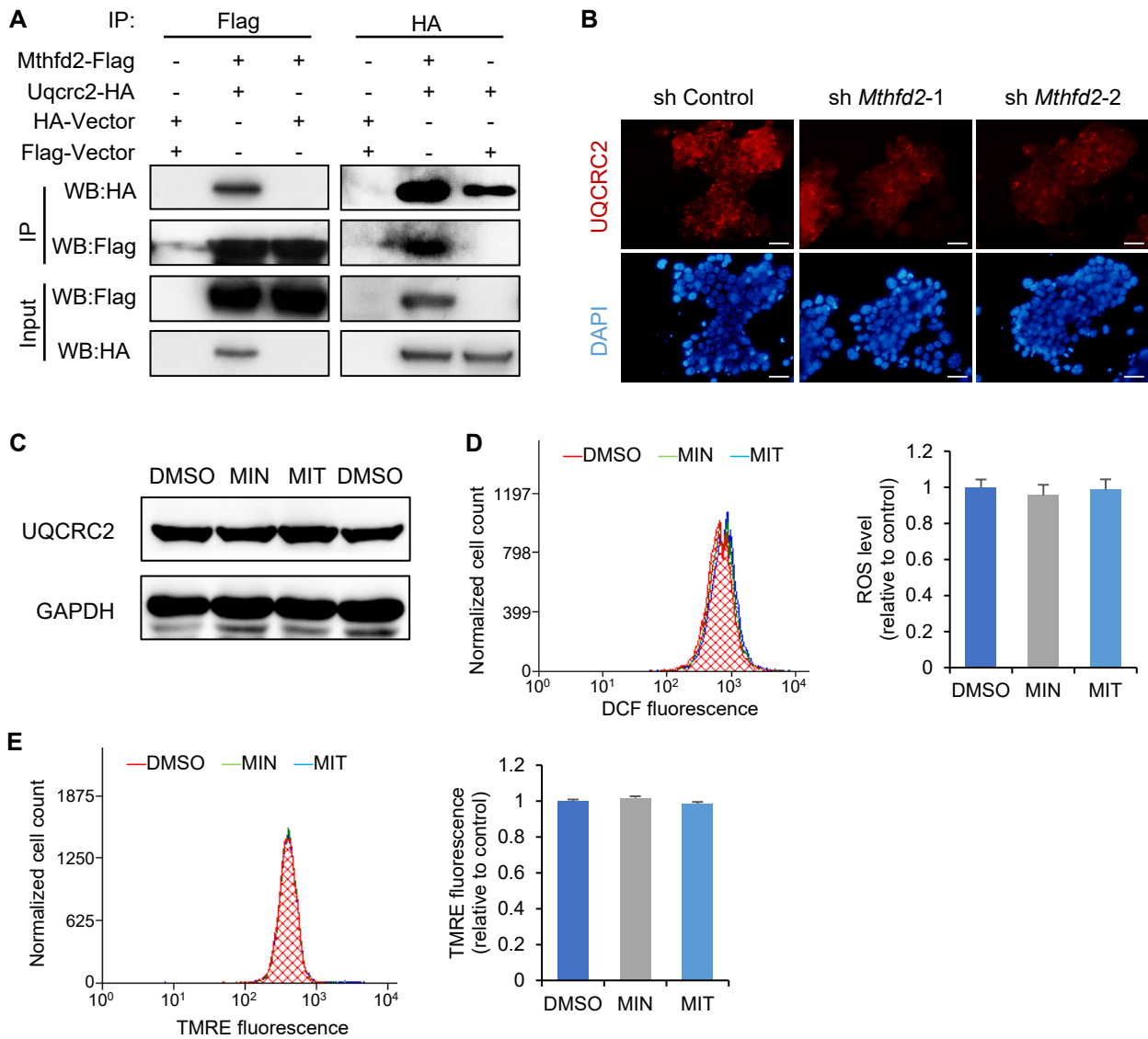
Figure S5. *Mthfd2* function in mESCs is Independent of Its Enzymatic Activity, Related to Figure 3 and 4.

(A) CO-IP results showing the specific interaction between exogenously expressed MTHFD2-Flag and UQCRC2-HA in mESCs. WB was conducted with the indicated antibodies.

(B) Immunofluorescence staining for UQCRC2 in *Mthfd2* KD mESCs. DAPI was used to indicate the nuclei. Scale bar, 50 μm.

(C) WB analysis of UQCRC2 protein level in MI-mESCs. GAPDH was used as a loading control.

(D) Flow cytometry analysis of ROS levels in MI-mESCs. A representative histogram (left) and quantification of the mean fluorescence intensity (MFI) (right) are presented.

(E) Measurements of the mitochondrial membrane potential in MI-mESCs using tetramethylrhodamine methyl ester (TMRE). A representative histogram (left) and quantification of the MFI (right) are presented.

Data are pooled from 3 independent experiments.

A

Down Term Top 10

positive regulation of transcription, DNA-templated
DNA repair
mRNA processing
ribosome biogenesis
rRNA processing
positive regulation of transcription from RNA polymerase II promoter
negative regulation of transcription from RNA polymerase II promoter
cellular response to DNA damage stimulus
transcription, DNA-templated
regulation of transcription, DNA-templated

Count number

B

FAN1
GTF2H3
TRIP13
ATM
NUCKS1
RECQL4
ERCC2
RAD52
HELQ
ORAOV1
CHEK2
TRP53
ERCC4
RPA2
LIG3
RNF168
GEN1
PARP9
DTX3L
SFPQ
ERCC3
RECQL5
AP5Z1
DNA2
DCLRE1C
RECQL
XRCC1
H2AFX
GTF2H2
YY1
HMGA1-RS1
LIG4
APEX1
HMGA1

shControl-1
shControl-2
sh*Mthfd2*-2-1
sh*Mthfd2*-2-2
sh*Mthfd2*-1-1
sh*Mthfd2*-1-2

C

Nucleus   Cytoplasm

β-Tubulin

Histone H3

D

IP

Input   MTHFD2   IgG

MTHFD2
CYC1
UQCRC2   WB
EXO1
CDK1

100μM MIN treated

E

CPT treated

sh Control   sh *Mthfd2*-1   sh *Mthfd2*-2

Caspase 3

DAPI

F

CPT treated

sh Control   sh *Mthfd2*-1   sh *Mthfd2*-2

MTHFD2

DAPI

G

CPT treated

sh Control   sh *Exo1*-1   sh *Exo1*-2

Caspase 3

DAPI

H

DMSO   MIN   MIT

P1

P4

γ-H2AX / DAPI

I

No. of γ-H2AX foci per cell

P1   P4

DMSO
MIN
MIT

Figure S6

Figure S6. *Mthfd2* Modulates HR Repair Regardless of Its Enzymatic Activity, Related to Figure 5 and 6.

(A) Top 10 of enriched GO terms potently downregulated by *Mthfd2*.

(B) Heat-map of DEGs about DNA repair between Control mESCs and *Mthfd2* KD mESCs.

(C) WB analysis of the distribution of the cytoplasm and nucleus extracts of mESCs. β-Tubulin and Histone H3 were used as loading controls for the cytoplasmic and nuclear proteins, respectively.

(D) CO-IP results showing the interactions between endogenous MTHFD2 and UQCRC2, CYC1, EXO1, CDK1 proteins in MIN-mESCs. WB was conducted with the indicated antibodies.

(E and F) IF staining for Caspase 3 (E) and MTHFD2 (F) in *Mthfd2* KD mESCs post-CPT treatment. DAPI was used to indicate the nuclei. Scale bar, 50 μm.

(G) IF staining for Caspase 3 in *Exo1* KD mESCs post-CPT treatment. DAPI was used to indicate the nuclei. Scale bar, 50 μm.

(H and I) IF staining for γ-H2AX in MI-mESCs. Representative images (H) and quantification of the average number of γ-H2AX foci per cell (I) (n = 50 nuclei) are shown. DAPI was used to indicate the nuclei. Scale bar, 50 μm. Data are pooled from 3 independent experiments (mean $\pm$ SEM). *$P < 0.05$, **$P < 0.01$, and ***$P < 0.001$ (Student's *t* test) compared to the control.
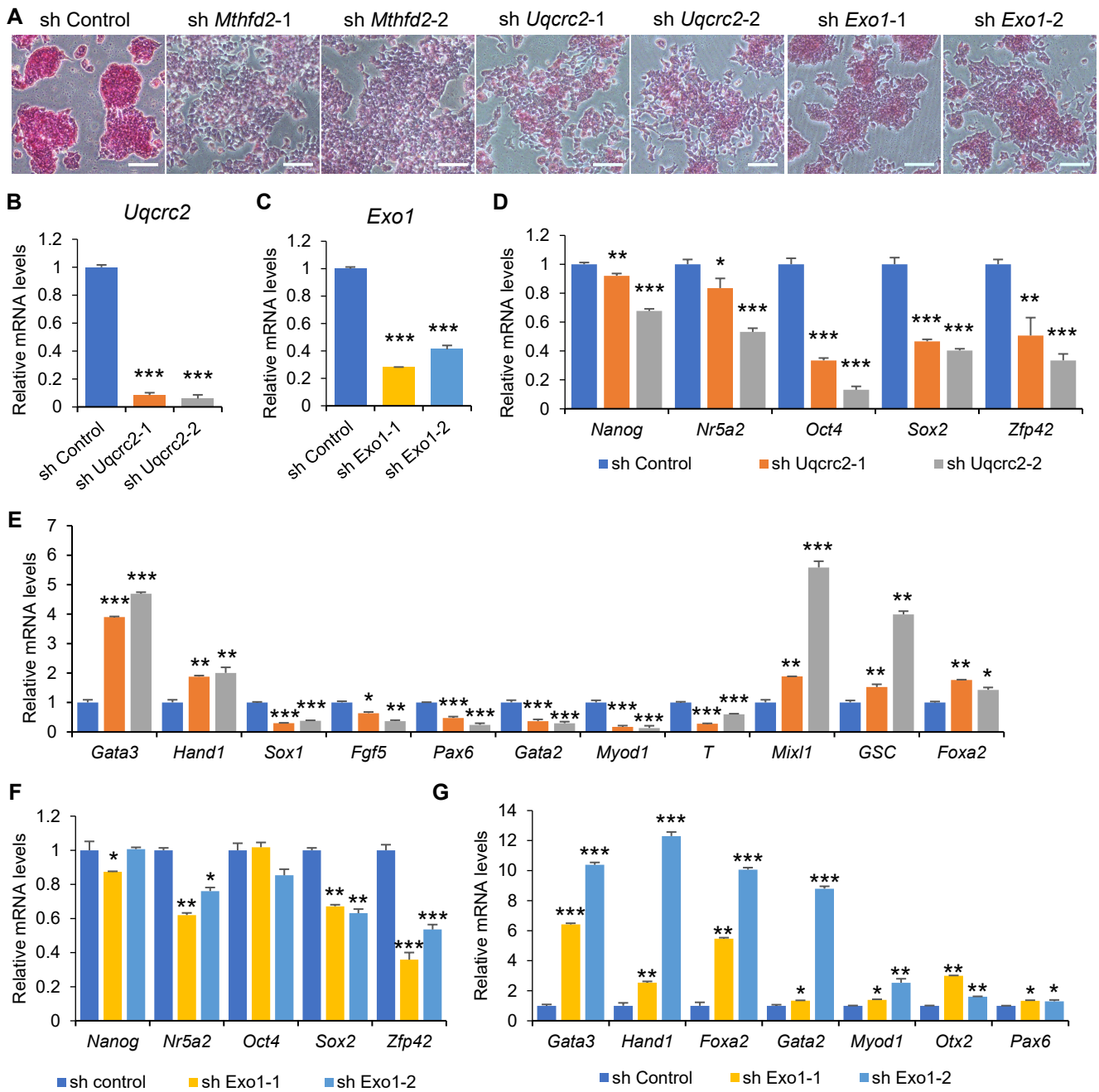
Figure S7. *Uqcrc2* or *Exo1* regulates mESC self-renewal, Related to Figure 7.

(A) Representative results of *Uqcrc2* KD mESCs and *Exo1* KD mESCs with AP staining. Scale bar, 100 μm.

(B and C) qRT-PCR analysis of mRNA levels of *Uqcrc2* and *Exo1* in the samples described in (A).

(D and E) qRT-PCR analysis of mRNA levels of pluripotency marker genes (D) and lineage marker genes (E) in *Uqcrc2* KD mESCs.

(F and G) qRT-PCR analysis of mRNA levels of pluripotency marker genes (F) and lineage marker genes (G) in *Exo1* KD mESCs.

Data (B-G) are pooled from 3 independent experiments (mean ± SD) relative to EF1-α and the control. $*P < 0.05$, $**P < 0.01$, and $***P < 0.001$ (Student's t test) compared to the control.

Table S4. The List of Overexpression Primer Sequences Used in This Study, Related to Figures 1-7.

The primers used for gene overexpression		
Gene	Forward Primer Sequence (5' to 3')	Reverse Primer Sequence (5' to 3')
Mthfd2	ATGGCTTCAGTTTCCTTGTTG	CTAGTTGGTGGCGACTCCG
Uqcrc2	ATGAAGCTCCTCAGCAGGG	TAACTCGTCGAGAAAAGG
Cdk1	ATGGAAGACTATATCAAAATAGAGAAAATTGG	CTACATCTTCTTAATCTGATTGTCC
The primers used for generation of Flag-tagged Mthfd2 plasmid		
Name of plasmid	Primer sequences (5' to 3')	
pCAG-Mthfd2-F	CGACGCGTATGGCTTCAGTTTCCTTGTTG	
pCAG-Mthfd2-Flag-R	CCTTAATTAACTACTTATCGTCATCGTCTTTGTAATCAATATCATGATCCTTGTAGTCTCCGTCGTGGTCCTTATAGTCGTTGGTGGCGACTCCG	
PB-Ubc-Mthfd2-F	CCCTCGAGATGGCTTCAGTTTCCTTGTTG	
PB-Ubc-Mthfd2-Flag-R	CGACGCGTCTACTTATCGTCATCGTCTTTGTAATCAATATCATGATCCTTGTAGTCTCCGTCGTGGTCCTTATAGTCGTTGGTGGCGACTCCG	
The primers used for generation of HA-tagged Uqcrc2 plasmid		
Name of plasmid	Primer sequences (5' to 3')	
pCAG-Uqcrc2-F	CGGGATCCATGAAGCTCCTCAGCAGGG	
pCAG-Uqcrc2-HA-R	CCTTAATTAATTAAGCGTAATCTGGAACATCGTATGGGTATAACTCGTCGAGAAAGG	
The primers used for GST pull down		
Gene	Forward Primer Sequence (5' to 3')	Reverse Primer Sequence (5' to 3')
Exo1	AAGGAAAAAGCGGCCGCATGGGGATTCAAGGGTTACT	CGGAATTCTTAGTGAAATATTGCTCTCTG
Cdk1	AAGGAAAAAGCGGCCGCATGGAAGACTATATCAAAATAGAGAAAATTGG	CGGAATTCCTACATCTTCTTAATCTGATTGTCCAAGTCA
Uqcrc2	AAGGAAAAAGCGGCCGCATGAAGCTCCTCAGCAGGG	CGCGGATCCTTATAACTCGTCGAGAAAGG
Cyc1	AAGGAAAAAGCGGCCGCATGGCGGCGGCGGCGGCTT	CGGAATTCTCACTTGGGTGGCCGATAA
Mthfd2	CGCGGATCCATGGCTTCAGTTTCCTTGTTG	AAGGAAAAAGCGGCCGCCTAGTTGGTGGCGACTCCG

Table S5. The List of shRNA and sgRNA Sequences Used in This Study, Related to Figures 1, 3-7.

The list of shRNA sequences	
Name of shRNA	shRNA sequences (5' to 3')
sh *Mthfd2*-1F	CGCGTCCCCGTCCAAACAGCGCGGAGTCTTCAAGAGAGACTCCGCGCT GTTTGGACTTTTTGGAAAT
sh *Mthfd2*-1R	CGATTTCCAAAAAGTCCAAACAGCGCGGAGTCTCTCTTGAAGACTCCGC GCTGTTTGGACGGGGA
sh *Mthfd2*-2F	CGCGTCCCCGCAGGCATTCCAACCTTAGGTTCAAGAGACCTAAGGTTGG AATGCCTGCTTTTTGGAAAT
sh *Mthfd2*-2R	CGATTTCCAAAAAGCAGGCATTCCAACCTTAGGTCTCTTGAACCTAAGGT TGGAATGCCTGCGGGGA
sh *Mthfd2*-3F	CGCGTCCCCGTGCCGATTGCAATGTTGCTTTCAAGAGAAGCAACATTGCA ATCGGCACTTTTTGGAAAT
sh *Mthfd2*-3R	CGATTTCCAAAAAGTGCCGATTGCAATGTTGCTTCTCTTGAAAGCAACATT GCAATCGGCACGGGGA
sh *Uqcrc2*-1F	GATCCCCGCTGTTGCCTTTCAGAATTCATTCAAGAGATGAATTCTGAAAG GCAACAGCTTTTTA
sh *Uqcrc2*-1R	AGCTTAAAAAGCTGTTGCCTTTCAGAATTCATCTCTTGAATGAATTCTGAA AGGCAACAGCGGG
sh *Uqcrc2*-2F	GATCCCCGCAGGTGGCTGAACAATTTCTTTCAAGAGAAGAAATTGTTCAG CCACCTGCTTTTTA
sh *Uqcrc2*-2R	AGCTTAAAAAGCAGGTGGCTGAACAATTTCTTCTCTTGAAAGAAATTGTTC AGCCACCTGCGGG
sh *Uqcrc2*-3F	GATCCCCGCTCTAGCTGCAGGTTCTTATTTCAAGAGAATAAGAACCTGCA GCTAGAGCTTTTTA
sh *Uqcrc2*-3R	AGCTTAAAAAGCTCTAGCTGCAGGTTCTTATTCTCTTGAAATAAGAACCTG CAGCTAGAGCGGG
sh *Exo1*-1F	GATCCCCGGATACCTACTGTTGGCTTCATTCAAGAGATGAAGCCAACAGT AGGTATCCTTTTTA
sh *Exo1*-1R	AGCTTAAAAAGGATACCTACTGTTGGCTTCATCTCTTGAATGAAGCCAAC AGTAGGTATCCGGG
sh *Exo1*-2F	GATCCCCGGGTCAAGCCGATTCTCATATTTCAAGAGAATATGAGAATCGG CTTGACCCTTTTTA
sh *Exo1*-2R	AGCTTAAAAAGGGTCAAGCCGATTCTCATATTCTCTTGAAATATGAGAATC GGCTTGACCCGGG
Sequences for generation of *Mthfd2* knockout plasmid		
	Forward Primer Sequence (5'to 3')	Reverse Primer Sequence (5'to 3')
Mthfd2-sgRNA-1	CACCGAGTTTCCTTGTTGTCTGCG T	AAACACGCAGACAACAAGGAAACT C
Mthfd2-sgRNA-2	CACCGCGGTTGTTGCGCCCCACG CA	AAACTGCGTGGGGCGCAACAACC GC
Sequences for check *Mthfd2* knockout		
Mthfd2-561	TGCCTTTCAGGGGTTCTC	AAGCGTCCGCATCTCCAC
Mthfd2-623	TTGGCCTAGCTGAGGGAC	GGGAGGAGGGAAGTTGGTA

Table S6. The List of qRT-PCR Primer Sequences Used in This Study, Related to Figures 1, 2 and 7.

Gene	Forward Primer Sequence (5'to 3')	Reverse Primer Sequence (5'to 3')
Mthfd2	CCTTGTTGTCTGCGTTGGCT	ATGACAACGGCTTCATTTCGCA
EF1α	GTGTTGTGAAAACCACCGCT	AGGAGCCCTTTCCCATCTCA
Exo1	TAAACACGTCGAGCCTGTCC	CAGAGCCCAGGAACCTTGTT
Uqcrc2	CCGGGTCCTTCTCGAGATTT	CTGCTTTAACGAACAAGCCGA
Cdk1	TAGACTTCCCAGCAGCCATTC	CACTTCCATCTGGGGGTCAT
Cyc1	ATCGTTCGAGCTAGGCATGG	GCCGGGAAAGTAAGGGTTGA
pMX-1811s	GACGGCATCGCAGCTTGGATACAC	
Oct4 Rv		CCAATACCTCTGAGCCTGGTCCGAT
Sox2 Rv		GCTTCAGCTCCGTCTCCATCATGTT
Klf4-943Rv		GTGGGTTAGCGAGTTGGA
c-Myc Rv		TCGTCGCAGATGAAATAGGGCTG
ex-Mthfd2		CCTGCTGTACTTCTTGCTTGATCTG
en-Oct4	AGTGGGGCGGTTTTGAGTAA	TTCCAAAGAGAACGCCCAGG
en-Sox2	GATCAGCATGTACCTCCCCG	TCCTCTTTTTGCACCCCTCC
Oct4	GGCGTTCTCTTTGGAAAGGTG	AGTTCGCTTTCTCTTCCGGG
Sox2	CCCACCTACAGCATGTCCTAC	AGTGGGAGGAAGAGGTAACCA
Klf4	GACTAACCGTTGGCGTGAGG	GTCTAGGTCCAGGAGGTCGT
Cdx2	AAGACAAATACCGGGTGGTG	CCAGCTCACTTTTCCTCCTG
Eomes	ACCGGCACCAAACTGAGA	AAGCTCAAGAAAGGAAACATGC
Esrrb	TTTCTGGAACCCATGGAGAG	AGCCAGCACCTCCTTCTACA
Fgf5	ATCTACCCGGATGGCAAAGT	TCTCGGCCTGTCTTTTCAGT
Foxa2	GAGCAGCAACATCACCACAG	CGTAGGCCTTGAGGTCCAT
GSC	AGTCAGAAAACGCCGAGAAG	TCGACTGTCTGTGCAAGTCC
Hand1	TCAAAAAGACGGATGGTGGT	GCGCCCTTTAATCCTCTTCT
Klf2	ACCAAGAGCTCGCACCTAAA	GTGGCACTGAAAGGGTCTGT
Nanog	TTCTTGCTTACAAGGGTCTGC	AGAGGAAGGGCGAGGAGA

Nr5a2	TGCTGAGCCCTGAAGCTATT	AGGGTTACTGCCCGTTTTCT
Otx2	AGAGGACGACATTTACTAGGGC	ATTCTTAAACCATACCTGCACC
Pax6	TACCAGTGTCTACCAGCCAAT	TGCACGAGTATGAGGAGGTCT
Zfp42	CAGTTCGTCCATCTAAAAAGGGAGG	TCTTAGCTGCTTCCTTGAACAATGCC
Sox1	ATACCGCAATCCCCTCTCAG	ACAACATCCGACTCCTCTTCC
Sox17	CTCGGGGATGTAAAGGTGAA	CTTTGGCCCACACCATAAAG
T	ATCAGAGTCCTTTGCTAGGTAG	GTTACAATCTTCTGGCTATGC
Tbx3	ATCGCCGTTACTGCCTATCA	TGCAGTGTGAGCTGCTTTCT
Gata3	CTTATCAAGCCCAAGCGAAG	CATTAGCGTTCCTCCTCCAG
Gata2	AGCTGCACAATGTTAACAGGC	AAGGGCGGTGACTTCTCTTG
Myod1	TACAGTGGCGACTCAGATGC	TAGTAGGCGGTGTCGTAGCC
Nodal	ACGTTCACCGTCATTCCTTC	GTAGGGCTGATGCCAACACT
Utf1	CTACGAGGTTCCTTCGACCA	GACTGGGAGTCGTTTCTGGA
KDR	ATGAATTGCCCTTGGATGAG	AGCGTCTGCCTCAATCACTT
Myf5	CCACCAACCCTAACCAGAGA	GTTCTCCACCTGTTCCCTCA
Mixl1	CCATGTACCCAGACATCCACT	CGGTTCTGGAACCACACCT
Acvr1b	GGCTCAGGGTTACCCCTTTT	TTCACGGAACCAAGACCGTT
Spry2	TCCACCGATTGCTTGGAAGT	CACATCTGAACTCCGTGATCG
Tdgf1	CTGCCCAAGAAGTGTTCCCTG	TCGTCACAGACGGCGTTTG
Bmp4	AGGAGGAGGAGGAAGAGCAG	CCTGGGATGTTCTCCAGATG
Nes	GATCGCTCAGATCCTGGAAG	AGGTGTCTGCAAGCGAGAGT

Table S7. Cell Proliferation of *Mthfd2* Knockdown Cells, Related to Figure 1.

First Experiment					
	Day1	**Day2**	**Day3**	**Day4**	
sh Control mESCs	3	29	98	266	x 10^4 cells
sh *Mthfd2*-1 mESCs	3	30.4	110	280	x 10^4 cells
sh *Mthfd2*-2 mESCs	3	28.6	100	270	x 10^4 cells
Second Experiment					
	Day1	**Day2**	**Day3**	**Day4**	
sh Control mESCs	2.4	15.2	68	224	x 10^4 cells
sh *Mthfd2*-1 mESCs	2.4	14	70	218	x 10^4 cells
sh *Mthfd2*-2 mESCs	2.4	13.4	67	210	x 10^4 cells
Third Experiment					
	Day1	**Day2**	**Day3**	**Day4**	
sh Control mESCs	2.6	24	92	210	x 10^4 cells
sh *Mthfd2*-1 mESCs	2.6	20	84.6	206	x 10^4 cells
sh *Mthfd2*-2 mESCs	2.6	22.4	88	220	x 10^4 cells

Supplemental Experimental Procedures

Key Resources Table

Reagent or Resource	Source	Identifier
Antibodies		
Mthfd2	Santa Cruz	sc-390709
Mthfd2	Abcam	ab151447
Nanog	Abcam	ab70482
Sox2	Abcam	ab97959
SSEA1	Abcam	ab16285
Nestin	Abcam	ab134017
β-Tubulin	Abcam	ab151318
Histone H3	EASYBIO	BE3021
Uqcrc2	Absin	abs116449
Cdk1	Absin	abs115034
Cyc1	Absin	abs104557
Exo1	Absin	abs140694a
Oct 3/4	Santa Cruz	SC-5279
α-Smooth Muscle Actin	Abcam	ab5694
Gata6	Abcam	ab22600
Gapdh	Cell Signaling Technology	2118L
GST	EASYBIO	BE2013
Caspase 3	Cell Signaling Technology	#9664s
HA	EASYBIO	BE2007
HA	EASYBIO	BE2008
Flag	EASYBIO	BE2004
Flag	EASYBIO	BE2005
gamma H2A.X	Abcam	ab11174
Mouse IgG	Beyotime	A7028

Rabbit IgG	Beyotime	A7016
Phospho-CDK Substrate Motif [(K/H) pSP]	Cell Signaling Technology	9477S
Rad51	Abcam	ab133534
Phospho-Threonine-Proline (P-Thr-Pro-101)	Cell Signaling Technology	9391S
Bacterial and Virus Strains		
pSuper-puro	Oligoengine	VEC-PBS-0008
pLVTHM	Addgene	12247
pMXs-Retroviral	Genome Institute of Singapore	N/A
pX330-Green	Massachusetts Institute of Technology	N/A
pCAG-IRES-puro	This paper	N/A
PB-Ubc-Neo	This paper	N/A
Chemicals, Peptides, and Recombinant Proteins		
Phosphatase Inhibitor Cocktail	Cell Signaling Technology	5870S
Protease Inhibitor Cocktail	Cell Signaling Technology	5871S
MG132	Selleck	S2619
Camptothecin	Selleck	S1288
Doxycycline	Sigma	D9891
Polybrene (Hexadimethrine bromide)	Sigma	107689
Critical Commercial Assays		
Alkaline Phosphatase Detection Kit	Millipore	SCR004
ATP Assay Kit	Beyotime	S0026B
TMRE-Mitochondrial Membrane Potential Assay Kit	Abcam	ab113852
Reactive Oxygen Species Assay Kit	Beyotime	S0033
Cell lysis buffer for Western and IP	Beyotime	P0013
Fast Silver Stain Kit	Beyotime	P0017S
Protein G Agarose	Roche	11243233001
ECL luminescence reagent	Sangon Biotech	C510043
MitoSOX Red Mitochondrial Superoxide Indicator	Yeasen	40778ES50
cycloheximide	MedChemExpress	HY-12320

Antimycin A	Biovision	2247-10
RO-3306	MedChemExpress	HY-12529
MIN	synthesis	N/A
MIT	synthesis	N/A
GelRed	Biotium	41003
Deposited Data		
RNA-sequence data	This paper	SRP149554
Microarray data	(Heng et al., 2010)	GSE19023
Microarray data	(Han et al., 2010)	GSE19164
RNA-sequence data	(Cao et al., 2014)	SRA076823
Experimental Models: Cell Lines		
E14	Genome Institute of Singapore	CRL-1821
G4	Mount Sinai Hospital	N/A
Experimental Models: Organisms/Strains		
Oct4-GFP (OG2) mice	Tongji University; National Institute of Biological Sciences	N/A
Rosa26-M2rtTA Col1a1-tetO-Pou5f1 (TF4) mice	(Gao et al., 2013)	N/A
Recombinant DNA		
pCAG-Mthfd2-puro plasmid	This paper	N/A
pCAG-Mthfd2-Flag-puro plasmid	This paper	N/A
Pb-Ubc-Mthfd2-Flag-Neo plasmid	This paper	N/A
pCAG-Uqcrc2-HA-puro plasmid	This paper	N/A
pSuper-Mthfd2-puro plasmid	This paper	N/A
pLVTHM-Mthfd2-GFP plasmid	This paper	N/A
pSuper-Uqcrc2-puro plasmid	This paper	N/A
pSuper-Cyc1-puro plasmid	This paper	N/A
pSuper-Exo1-puro plasmid	This paper	N/A
pMXs-Oct4 plasmid	(Takahashi and Yamanaka, 2006)	N/A
pMXs-Sox2 plasmid	(Takahashi and Yamanaka, 2006)	N/A
pMXs-Klf4 plasmid	(Takahashi and Yamanaka, 2006)	N/A

pMXs-Mthfd2 plasmid	This paper	N/A
pCAG-Uqcrc2-Neo plasmid	This paper	N/A
pCAG-Cdk1-Neo plasmid	This paper	N/A
pCAG-Mthfd2-Neo plasmid	This paper	N/A
pET-28a (+) (Uqcrc2)	This paper	N/A
pET-28a (+) (Cdk1)	This paper	N/A
pET-28a (+) (Cyc1)	This paper	N/A
pET-28a (+) (Exo1)	This paper	N/A
pGEX-4T-1 (Mthfd2)	This paper	N/A
Software and Algorithms		
Summit 5.2	Beckman Coulter	N/A
Trimmomatic	(Bolger et al., 2014)	N/A
Hisat2 2.1.0	(Kim et al., 2015)	N/A
HT-seq 0.61	(Anders et al., 2015)	N/A
DESeq2 1.18.1	R package (Love et al., 2014)	N/A
GOstats 2.44.0	R package (Falcon and Gentleman, 2007)	N/A
Mascot 2.4	Matrix Science	N/A
CASP comet assay software	Andor Technology	N/A

Contact for Reagent and Resource Sharing

Further information and requests for reagents should be directed to and will be fulfilled by the Lead Contact, Dr. Jianyong Han (hanjy@cau.edu.cn).

Experimental Procedures

Animal Experiments

All animal studies proceeded according to the guidelines of the Institute Animal Care and Use Committee and were approved by the Animal Care and Use Committee of China Agricultural University. We used CD1 (ICR) mice as the embryo donors and recipients, which were purchased from Beijing Vital River Laboratory Animal Technology Co., Ltd. (Beijing, China). All mice were maintained in specific pathogen-free (SPF) conditions with a 12 h dark/12 h light cycle.

Cell Culture and Transfection.

For G4 and E14 mESCs, Leukemia inhibitory factor (LIF) and serum culture medium were used to maintain mESCs self-renewal. The serum + LIF mESCs medium contained DMEM with 15% fetal bovine serum (FBS), 1% GlutaMAX, 1% sodium pyruvate, 1% nonessential amino acids (NEAA), 0.1 mmol/L β-mercaptoethanol, 1% penicillin/streptomycin (all from Gibco) and 1000 units/mL mouse Leukemia Inhibitory Factor (mLIF, Miltenyi Biotec).

To detect the developmental potential of iPSCs by 8-cell-stage embryo injection and tetraploid complementation, the OSKM2 iPSCs were cultured in 2i+LIF mESCs medium. The 2i+LIF mESCs medium contained DMEM with 15% FBS, 1% GlutaMAX, 1% sodium pyruvate, 1% NEAA, 0.1 mmol/L β-mercaptoethanol, 1% penicillin/streptomycin, 1000 units/mL mLIF, 1 μM PD0325901 (4423, Tocris), and 3 μM CHIR99021 (4192, Tocris).

The MEF cells were maintained on Gelatin in MEF medium, which contained DMEM with 10% FBS, 1% GlutaMAX, 1% NEAA and 1% penicillin/streptomycin.

Plat-E packaging cells (Cell Biolabs), which were used to produce retrovirus, were maintained in MEF medium. All cells were cultured in a humidified incubator at 37°C and 5% CO_2.

Transfection of plasmids into mESCs and MEF cells and Plat-E packaging cells was performed using Lipofectamine 3000 (Invitrogen).

Construction of Vectors

In order to overexpress the candidate protein, the coding sequence of full-length mouse candidate genes was cloned into the pMXs retroviral vector, pCAG-IRES-puro vector or PB-Ubc-neo vector. The sequences of primers are showed in Table S4.

The short hairpin RNA (shRNA) targeting mouse *Mthfd2* mRNA or other genes and the control shRNA was cloned into pSuper-puro Vector (Oligoengine). The sequences of shRNA are showed in Table S5. The sgRNAs for *Mthfd2* were designed by using the website provided by Zhang Feng laboratory (https://zlab.bio/guide-design-resources). The sequences of sgRNA are showed in Table S5. Then the sgRNA sequence was cloned into the pX330-Green vector.

Generation of Gene Knockdown Cells

The pSuper-puro plasmid was transfected into mESCs by Lipofectamine 3000. 24 h later, the mESCs were selected with 2 μg/mL of puromycin for 4 days. All those cells were cultured in serum + LIF mESCs medium.

Generation of Homozygous Knockout Cells

The mESCs were electroporated with pX330-Mthfd2-Green plasmid or pX330-Green control plasmid and cultured in serum + LIF mESCs medium. The plasmid was transiently expressed in cells by electroporation. 3 days later, the GFP-positive cell population were sorted by flow cytometry, and cultured in serum + LIF mESCs medium. Then colonies were picked and dissociated into single cells by TrypLE (Invitrogen). Most cells were cultured to obtain the stable *Mthfd2* KO cell lines, few remaining cells were lysed by Embryonic Cell Lysis Solution (CAT#:130806-1, TIANDZ). The Embryonic Cell Lysis Solution can be used to lyse 2-8 cells, and the lysate can be directly used for PCR. The knockout regions of those cells were amplified by PCR using primers (Table S5) and sequenced. By aligning with the wild type sequence, homozygous knockout cell clones were identified. According the previous reports that Mthfd2 may have an impact on cell proliferation in cancer cell, we prefer to pick the slow-growing colonies. The mESCs electroporated with pX330-Green control plasmid were used as the control cells.

Derivation of Mouse Embryonic Fibroblast Cells (MEFs)

MEFs were isolated from 13.5-day embryos heterozygous for the Oct4-GFP/OSKM transgenic allele. Isolated MEFs in early passages (up to passage 4) were used for further experiments.

Induction of Pluripotent Stem Cells

For iPSCs induction, pMXs retroviral vectors containing coding sequences of mouse *Oct4*, *Sox2*, *Klf4* and candidate genes cDNAs were cotransfected into Plat-E cells using Lipofectamine 2000 (Invitrogen). Culture medium containing virus particles was collected at 24 or 48 h after transfection and filtered through a 0.22 μm filter. MEF cells were infected with equal amounts of OSK and candidate genes viruses mixed with 8 μg/mL polybrene (Sigma-Aldrich). After two rounds of infection, infected cells were changed to serum + LIF mESCs medium or KOSR medium (DMEM supplemented with 10% KnockOut SR XenoFree CTS (KOSR), 1% GlutaMAX, 1% sodium pyruvate, 1% NEAA, 0.1 mmol/L β-

mercaptophenol, 1% penicillin/streptomycin and 1000 units/mL mLIF). The medium was replaced daily. For quantification of reprogramming efficiency using the Oct4-GFP reporter, the transfected MEFs were scanned under a fluorescence microscope in Biostation (Nikon) on day 16 and scored for GFP$^+$ colonies. On day 18, cells were fixed and stained for alkaline phosphatase activity using an alkaline phosphatase detection kit (Millipore).

Embryoid Body and Teratoma Formation

The iPSCs were grown to approximately 80% confluence and dissociated into single cells in the differentiation medium (DMEM supplemented with 15% FBS, 1% GlutaMAX, 1% NEAA, 0.1 mmol/L β-mercaptophenol). They were seeded at a density of 1×10^5 cells per uncoated 3.5 cm Petri dish. The dishes were taped to a rotary platform in the incubator. Medium was changed every 2 days. Embryoid bodies were collected on day 7 for further differentiation on the uncoated Petri dishes in the differentiation medium.

Approximately 1×10^6 iPSCs were suspended in 150 μL DPBS and injected into NOD-SCID mice to form teratomas. Four weeks after injection, the teratomas were harvested, fixed overnight with 4% paraformaldehyde, embedded in paraffin, sectioned, HE stained, and analyzed.

Production of Chimeric Mice

15-20 iPSCs (with a C57/BL6 background) were injected into an 8-cell stage embryo which was obtained from superovulated female CD1 mice. The reconstructed embryos were cultured *in vitro* and developed into blastocysts. Chimeras were produced by transplantation of injected blastocysts into uterus of pseudopregnant CD1 mice.

Tetraploid Embryo Complementation

The generation of mice by tetraploid embryo complementation was performed using previously described methods (Zhao et al., 2009). Briefly, two-cell embryos were collected from the oviducts of CD-1 females (white coat color) and electrofused by Electro cell manipulator (ECM 2001, BTX Harvard Apparatus) to produce one-cell tetraploid embryos that were then incubated in KSOM until the blastocyst stage. 15-20 iPSCs were injected into each tetraploid blastocyst and approximately 10-14 embryos were transferred to CD-1 pseudopregnant recipient females. All the embryos and live pups

derived from tetraploid blastocyst injection were male, since the injected iPSCs or mESCs were originated from male mice.

Identification of Cell Proliferation

Cells were plated at 2×10^4 cells/well in 12-well plates to examine growth curves. The cells were washed with DPBS, treated with TrypLE, and counted with a LUNA Automated Cell Counter at the indicated times to identify their proliferation.

RNA Purification and cDNA Preparation

Total RNA was extracted from cells using RNeasy Mini Kit (QIAGEN) according to the manufacturer's instructions. The RNA was reverse-transcribed using oligo-dT and M-MLV Reverse Transcriptase (Promega).

Quantitative Real-Time PCR

Quantitative Real-Time PCR (qRT-PCR) was run on a Light Cycler 480 II Real-Time PCR System (Roche) using the Light Cycler 480 SYBR Green I Master (Roche). The data was analyzed using the comparative CT ($2^{-\Delta\Delta CT}$) method. The ΔCT was calculated using EF1-α or Gapdh as internal control. All experiments were performed more than three biological replicates. Primer sequences were provided in Table S6.

Immunofluorescence Staining

For immunofluorescence (IF) staining, cells were fixed with 4% paraformaldehyde (PFA) for 30 min at room temperature, permeabilized with 0.5% Triton X-100 for 30 min, blocked with PBS containing 5% BSA (Sigma) for 2 h. The cells were then stained with primary antibodies against Oct4 (Santa Cruz SC-5279), Sox2 (Abcam ab97959), Nanog (Abcam ab70482), SSEA1 (Abcam ab16285), Nestin (Abcam ab134017), Gata6 (Abcam ab22600), α-Smooth Muscle Actin (Abcam ab5694), Mthfd2 (Abcam ab151447) at 4°C overnight, followed by staining with the respective secondary antibodies conjugated to Alexa Fluor (Invitrogen). For nuclear staining, the cells were counterstained with DAPI (Sigma) for 5 min.

Western Blot Analysis

Cell extracts were prepared in lysis buffer (20 mM Tris-HCl pH 7.5, 80 mM NaCl, 2 mM EDTA, 10% glycerol, 0.2% NP-40) supplemented with the PIC and phosphatase inhibitor cocktail. Protein concentration was determined with a Bradford Protein Assay Kit (Bio-Rad). Cell lysates were boiled for 5 min and the equal amounts of denatured protein samples were separated by SDS-PAGE gel and transferred to Immobilon PVDF 0.2 mm membranes (Millipore). Membranes were blotted with 5% non-fat milk prepared in Tris-buffer saline-plus 0.1% Tween-20 (TBST) at room temperature for 1 h and then incubated with primary antibodies diluted in 5% non-fat milk overnight at 4°C, followed by the treatment with horseradish peroxidase (HRP)-conjugated secondary antibodies for 1 h on the next day. After washing with TBST three times, the blotted membranes were exposed with ECL luminescence reagent (Sangon Biotech). For protein degradation assays, 24 h after control and *Mthfd2* shRNA transfection, mESCs were treated with 2ug/mL puromycin for 48h-72h and then treated with 10 mM MG132 (Selleck) for 3 h before harvest(Zhu et al., 2017). The following antibodies were used for western blotting: Mthfd2(Santa Cruz sc-390709; Abcam ab151447), Oct4 (Santa Cruz SC-5279), Gapdh (Cell Signaling Technology 2118L), β-tubulin (Abcam ab151318), Uqcrc2 (Absin abs116449), Cyc1 (Absin abs104557), Cdk1 (Absin abs115034), Exo1 (Absin abs140694a), HA (EASYBIO BE2007-100; EASYBIO BE2008-100), FLAG (EASYBIO BE2004-100; EASYBIO BE2005-100), Phospho-CDK Substrate Motif [(K/H)pSP] (Cell Signaling Technology 9477S), Phospho-Threonine-Proline (P-Thr-Pro-101) (Cell Signaling Technology 9391S). All antibodies were used at the recommended concentration.

Generation of Mthfd2-Flag mESCs and Uqcrc2-HA mESCs

To establish a mESC line stably expressing Mthfd2-Flag, mESCs were electroporated with 4PB (transposase) and the pCAG-Mthfd2-Flag-puro plasmid or PB-Ubc-Mthfd2-Flag-neo plasmid which carried a sequence of Mthfd2 fused with 3xFlag at its C-terminal. Then, the mESCs were selected with 2 μg/mL of puromycin for 4 days or 0.5 mg/mL of G418 for one week. Similarly, to establish a mESC line stably expressing Uqcrc2-HA, mESCs were electroporated with 4PB (transposase) and the pCAG-Uqcrc2-HA-puro plasmid which carried a sequence of Uqcrc2 fused with HA at its C-terminal. Then, the mESCs were selected with 0.5 mg/mL of G418 for one week. All those cells were cultured in serum + LIF mESCs medium.

Subcellular Fraction Isolation

Control and Mthfd2-Flag mESCs cultured in 100 mm petri dishes were washed twice by DPBS, cells were scraped and added 5 mL lysis buffer (10 mM HEPES-NaOH pH 7.9, 10 mM KCl, 1.5 mM $MgCl_2$, and 0.5 mM b-mercaptoethanol supplemented with Protease Inhibitor Cocktail (PIC) and phosphatase inhibitor cocktail), vortex shortly, and incubated on ice for 20 min. Then the cell lysate was supplemented with 100 μL of 10% NP-40, vortex shortly, incubated on ice for 1 min, and centrifuged at 16,000g for 10 min. The supernatant was kept as cytoplasmic proteins, and the pellet was used for nuclear protein extraction. Next, the pellet was washed twice by cold DPBS (2 mL/each), then treated by 1 mL of the nuclei lysis buffer (10 mM Tris-HCl, pH 7.6, 420 mM NaCl, 0.5% NP-40, 1 mM DTT, 1 mM PMSF, 2 mM $MgCl_2$ plus PIC and phosphatase inhibitor cocktail), and dispersed by tips and incubated on ice for 40 min, followed by vortex every 5 min. The lysate was centrifuged at 16,000g for 15 min, the supernatant was kept as nuclear proteins (before proceeding to IP assays, 1 mL of lower salt buffer consisting of 10 mM Tris-HCl, pH 7.6, 1 mM DTT, 1 mM PMSF, 2 mM $MgCl_2$ plus PIC and phosphatase inhibitor cocktail was added to adjust the concentration of NaCl to 210 mM). The separated subcellular fractions were used for further assays and analysis.

GST pull down

The bacteria were grown in sterile lysogeny broth (LB) medium with constant swirling (37°C, 180 r/min). After about 3 h, the bacteria were transferred to 500 mL sterile LB medium and incubated at the same condition to the exponential growth phase that measured as the OD600. The expression of interest proteins was induced with IPTG at a final concentration of 1 mM. The bacteria were incubated overnight in a shaker at 16°C. The next morning, the bacteria were centrifuged (3500 r/min, 4°C, 15 min) to pellet the bacteria.

To purify protein, the bacteria pellet was re-suspended in lysis buffer and lysed by sonication on ice for maintaining lower temperature. Then the lysate was centrifuged at 18400 r/min for 45 min at 4°C. Obtained supernatant was purified using a Ni^{2+} affinity chromatography column. Finally, both the precipitation after sonication and the purified proteins were detected by 12% SDS-PAGE.

Briefly, 0.5 mg of His-Uqcrc2/Cyc1/Exo1/Cdk1 fusion proteins in 1000 mL GST binding buffer (250 mM NaCl, 40 mM Tris-HCl, pH 7.5, 0.1 mM EDTA, 10% glycerol, 0.1% Triton X-100, 1 mM DTT, 0.1 mM PMSF, 0.1 mg/mL BSA) were exposed to GST conjugated Mthfd2 at 4°C for more than 1.5 h,

followed by three times of warm wash using GST binding buffer. Finally, conjugated proteins were eluted by SDS loading buffer boiling at 100°C for 10 min, and examined by western blot analysis.

Intracellular Lactate and Glucose Content Measurement

Intracellular glucose content and lactate accumulation of Control mESCs, *Mthfd2* KD mESCs and *Uqcrc2* KD mESCs were measured after 48 h of culture. Intracellular glucose contents were measured using Liquid chromatography-mass spectrometry (LC-MS). Intracellular lactate accumulations were measured using Gas chromatography-mass spectrometry (GC-MS).

Measurement of ROS and Mitochondrial Superoxide Measurement

For measurement of mitochondrial superoxide, cells were washed with DPBS and dissociated into single cells by TrypLE, and counted with a LUNA Automated Cell Counter. The same number of cells were used for subsequent detection.

For measurement of complete intracellular ROS, 2′,7′-dichloro uorescine diacetat (DCFH-DA, Beyotime) were mixed with dilution buffer HBSS and distributed evenly into each sample tube. Cells were incubated with 50 μM DCFH-DA for 30 min at 37°C (protected from light), mixed upside down every 5 min (protected from light). Cells were washed 3 times with DPBS, resuspended in DPBS and analyzed by flow cytometry on a Moflo-XDP (Beckman). The fluorescence values of 50,000 cells were analyzed for each sample. Fluorescence readings were normalized to cell number. The experiments were repeated three times independently. Data were analyzed as mean fluorescence intensity using summit 5.2 software.

For measurement of mitochondrial superoxide, MitoSOX Red Indicator (Yeasen) were mixed with dilution buffer HBSS and distributed evenly into each sample tube. Cells were incubated with 5 μM MitoSOX Red Indicator for 30 min at 37°C (protected from light), mixed upside down every 5 min (protected from light). Cells were washed 3 times with DPBS, resuspended in DPBS and analyzed by flow cytometry on a Moflo-XDP (Beckman). The fluorescence values of 50,000 cells were analyzed for each sample. Fluorescence readings were normalized to cell number. The experiments were repeated three times independently. Data were analyzed as mean fluorescence intensity using summit 5.2 software.

Mitochondrial Membrane Potential Measurement

For measurement of mitochondrial membrane potential, cells were washed with DPBS and dissociated into single cells by TrypLE, and counted with a LUNA Automated Cell Counter. The same number of cells were used for subsequent detection. Tetramethylrhodamine ethyl ester (TMRE, Abcam) were mixed with dilution buffer HBSS and distributed evenly into each sample tube. Cells were incubated with 50nM TMRE for 30 min at 37°C (protected from light), mixed upside down every 5 min (protected from light). Cells were washed 3 times with DPBS, resuspended in DPBS and analyzed by flow cytometry on a Moflo-XDP (Beckman). The fluorescence values of 50,000 cells were analyzed for each sample. Fluorescence readings were normalized to cell number. The experiments were repeated three times independently. Data were analyzed as mean fluorescence intensity using summit 5.2 software.

Intracellular ATP Measurement

Intracellular ATP levels were measured using the ATP assay kit (Beyotime) according to the manufacturer's instructions. Cells in 6-well plates were harvested and incubated with 200 µL lysis buffer, centrifuged at 4°C, 12,000g for 5 min. The supernatants were taken for subsequent determination. Add 100 µL ATP detection buffer to each hole of 96-well plate, place it at room temperature for 3-5 min, add 20 µL sample and mixed it quickly, then use luminometer to measure RLU value. The concentration of ATP in the sample was calculated according to the standard curve. Relative ATP levels were normalized to protein concentrations.

Drug Treatments

Cells were treated with 1 µM of Camptothecin (CPT, Selleck) for the indicated periods of time to induce DNA damage. Cells were treated with 10 µM MG132 (Selleck) for 4 h to block proteasomal degradation of Uqcrc2. Cells were treated with 100 µg/mL Cycloheximide (CHX, MedChemExpress) to inhibit protein synthesis, 0.5 µM antimycin A (Biovision) to inhibit mitochondrial electron transport chain complex III activity, 9 µM RO-3306 (MedChemExpress) to inhibit Cdk1 activity, 100 µM MIN or 100 µM MIT to inhibit Mthfd2 activity.

DNA Repair Kinetics Assay

For quantifying DSB repair kinetics, cells were treated with 1 µM CPT for 2 h after which the media was replaced with CPT-free media. Cells were immunostained with γ-H2AX antibody (Abcam ab11174) at

different time points post-CPT treatment, as described previously (Mukherjee et al., 2012). To stain for Rad51 foci, cells were treated with 1 μM CPT for 4 h. The cells were fixed with 4% paraformaldehyde/PBS and permeabilized with 0.5% Triton-X/PBS before incubation with antibodies. To obtain clear Rad51 foci, cells were subject to in situ fractionation (Cuadrado et al., 2006). The average number of γ-H2AX foci or Rad51 foci per nucleus was determined after scoring at least 50 nuclei.

Alkaline Comet Assay

Comet assay (alkaline condition) was performed as described (Swain and Subba Rao, 2011; Tice et al., 2000). Briefly, cells were trypsinized and resuspended in ice-colded PBS (Ca^{2+} and Mg^{2+} free) in a concentration of 1×10^5 cells/mL. An aliquot of 30 μL cells was added to 70 μL of 0.7% low-melting agarose kept at 37°C. The cell-agarose suspension was immediately pipetted and evenly spread onto an area of the comet slides. Slides were kept at 4°C for 10 min followed by immersion in lysis buffer (2.5 M NaCl, 100 mM Na_2EDTA, 10 mM Tris-base, 1% N-lauroylsarcosine, 1% Triton X-100, pH 10.0) for 1 hr at 4 °C in the dark. Slides were then removed, washed, and incubated in cold electrophoresis buffer (300 mM NaOH, 1 mM EDTA, pH > 13) for 30 min. Electrophoresis was carried out at 1 V/cm, 300 mA for 30 min in the dark at 4°C. At the end of the electrophoresis, the slides were washed with neutralization buffer (0.4 M Tris-HCl, pH 7.4) and immersed in ice-colded 100% ethanol at room temperature for 1 h and air dried. Slides were stained with GelRed (Biotium) for 30 min and immediately analyzed. Comets were analyzed by CASP comet assay software (Andor Technology). 50 cells were counted per slide.

Quantification and Statistical Analysis

RNA sequencing analysis

Total RNA was extracted from control mESCs and *Mthfd2* KD mESCs by RNeasy Mini Kit (QIAGEN). To construct and sequence the RNA-seq libraries, we used a polyA selection protocol according to the Illumina TruSeq RNA-Seq library protocol to construct RNA-Seq libraries. RNA-seq library was constructed for each RNA sample, which would make two biological replicates from each sample. Each library was sequenced using an Illumina Hiseq 2500 platform (150 bp pair-end reads). The low-quality reads and adaptor sequences were trimmed with Trimmomatic (Bolger et al., 2014). Clean reads were

aligned to mm10 Hisat2 (Kim et al., 2015). Gene expression levels were calculated by counting the overlap of reads on each gene with HT-seq (Anders et al., 2015) and normalized as RPKM with gene annotation file from Ensembly (release 87) and DESeq2 package in R (Love et al., 2014). Besides, differentially expressed genes were identified by DESeq2 package too. Functional enrichment for Gene Ontology (GO) and KEGG were performing with GOstats package (Falcon and Gentleman, 2007).

Immunoprecipitation and Mass Spectrometry Analysis

3 mg of cytoplasmic and nuclear proteins of control or Mthfd2-Flag mESCs were incubated with 12 μg of Flag antibody at 4°C overnight. Protein G agarose beads (Roche) in 1.5 mL were used to pull down Flag antibody precipitated proteins at 4°C for 1 h, following by washing three times with the lysis buffer and eluting in elution buffer (PH 2.7). The eluted mixture was separated by SDS-PAGE and stained by fast silver stain kit (Beyotime) for identify protein piece. Then the eluted mixtures were sent to analyzed by liquid chromatography-mass spectrometry (LC–MS).

The LC–MS samples were separated on a 2 cm C18 stationary phase column (Phenomenex, USA). While reaching the flow rate of 2 μL/min, the pump flow was split. Then, peptides were separated using a gradient elution that consisted of (a) 0.1% formic acid, (b) 0.1% formic acid in acetonitrile from 1% to 40% surpassing 95 min. Nanospray ESI-MS was performed on a Thermo Q-Exactive high resolution mass spectrometer (Thermo Scientific, USA). The ESI needle voltage was applied to 2 kV, and the isolation width was 4 Da. Raw data from the mass spectrometer were preprocessed with Mascot Distiller 2.4 for peak picking. The resulted peak lists include Mthfd2 and the Mthfd2-Flag samples were searched against Swissprot database using Mascot 2.4 search engine. After filtering the contamination, specific proteins were picked up against the negative control and annotated with UniProt database. Functional enrichment for Gene Ontology (GO) and KEGG were performing with GOstats package (Falcon and Gentleman, 2007). Finally, a potential regulatory network was constructed by Cytoscape.

Statistical analysis

The values reported in the graphs are presented as the mean ± SD or mean ± SEM. Student's *t* test was used to compare treatment groups. For all analyses, a p value less than 0.05 was considered statistically significant. Statistical significance is displayed as *P < 0.05, **P < 0.01, and ***P < 0.001*.

Additional Resources

The SRA website contains detailed data of RNA-seq experiments used in this study:

https://www.ncbi.nlm.nih.gov/sra/

Table S1. Microarray Data Analysis and Candidate Gene List, Related to Figures 1 and 2.

Table S2. RNA-Seq data of *Mthfd2* KD mESCs, Related to Figures 3 and 5.

Table S3. List of MTHFD2-Interacting Proteins, Related to Figures 3 and 5.

References

Anders, S., Pyl, P.T., and Huber, W. (2015). HTSeq--a Python framework to work with high-throughput sequencing data. Bioinformatics *31*, 166-169.

Bolger, A.M., Lohse, M., and Usadel, B. (2014). Trimmomatic: a flexible trimmer for Illumina sequence data. Bioinformatics *30*, 2114-2120.

Cao, S., Han, J., Wu, J., Li, Q., Liu, S., Zhang, W., Pei, Y., Ruan, X., Liu, Z., Wang, X., et al. (2014). Specific gene-regulation networks during the pre-implantation development of the pig embryo as revealed by deep sequencing. BMC Genomics *15*, 4.

Cuadrado, M., Martinez-Pastor, B., Murga, M., Toledo, L.I., Gutierrez-Martinez, P., Lopez, E., and Fernandez-Capetillo, O. (2006). ATM regulates ATR chromatin loading in response to DNA double-strand breaks. J. Exp. Med. *203*, 297-303.

Falcon, S., and Gentleman, R. (2007). Using GOstats to test gene lists for GO term association. Bioinformatics *23*, 257-258.

Gao, S., Wang, Z.L., Di, K.Q., Chang, G., Tao, L., An, L., Wu, F.J., Xu, J.Q., Liu, Y.W., Wu, Z.H., et al. (2013). Melatonin improves the reprogramming efficiency of murine-induced pluripotent stem cells using a secondary inducible system. J. Pineal Res. *55*, 31-39.

Han, J., Yuan, P., Yang, H., Zhang, J., Soh, B.S., Li, P., Lim, S.L., Cao, S., Tay, J., Orlov, Y.L., et al. (2010). Tbx3 improves the germ-line competency of induced pluripotent stem cells. Nature *463*, 1096-1100.

Heng, J.C., Feng, B., Han, J., Jiang, J., Kraus, P., Ng, J.H., Orlov, Y.L., Huss, M., Yang, L., Lufkin, T., et al. (2010). The nuclear receptor Nr5a2 can replace Oct4 in the reprogramming of murine somatic cells to pluripotent cells. Cell Stem Cell *6*, 167-174.

Kim, D., Langmead, B., and Salzberg, S.L. (2015). HISAT: a fast spliced aligner with low memory requirements. Nat. Methods *12*, 357-360.

Love, M.I., Huber, W., and Anders, S. (2014). Moderated estimation of fold change and dispersion for RNA-seq data with DESeq2. Genome Biol. *15*, 550.

Mukherjee, B., Tomimatsu, N., Amancherla, K., Camacho, C.V., Pichamoorthy, N., and Burma, S. (2012). The dual PI3K/mTOR inhibitor NVP-BEZ235 is a potent inhibitor of ATM- and DNA-PKCs-mediated DNA damage responses. Neoplasia *14*, 34-43.

Swain, U., and Subba Rao, K. (2011). Study of DNA damage via the comet assay and base excision repair activities in rat brain neurons and astrocytes during aging. Mech. Ageing Dev. *132*, 374-381.

Takahashi, K., and Yamanaka, S. (2006). Induction of pluripotent stem cells from mouse embryonic and adult fibroblast cultures by defined factors. Cell *126*, 663-676.

Tice, R.R., Agurell, E., Anderson, D., Burlinson, B., Hartmann, A., Kobayashi, H., Miyamae, Y., Rojas, E., Ryu, J.C., and Sasaki, Y.F. (2000). Single cell gel/comet assay: guidelines for in vitro and in vivo genetic toxicology testing. Environ. Mol. Mutagen. *35*, 206-221.

Zhao, X.Y., Li, W., Lv, Z., Liu, L., Tong, M., Hai, T., Hao, J., Guo, C.L., Ma, Q.W., Wang, L., et al. (2009). iPS cells produce viable mice through tetraploid complementation. Nature *461*, 86-90.

Zhu, Z., Li, C., Zeng, Y., Ding, J., Qu, Z., Gu, J., Ge, L., Tang, F., Huang, X., Zhou, C., et al. (2017). PHB Associates with the HIRA Complex to Control an Epigenetic-Metabolic Circuit in Human ESCs. Cell Stem Cell *20*, 274-289 e277.